Cell Reports

Compromised Survival of Cerebellar Molecular Layer Interneurons Lacking GDNF Receptors GFRα1 or RET Impairs Normal Cerebellar Motor Learning

Graphical Abstract

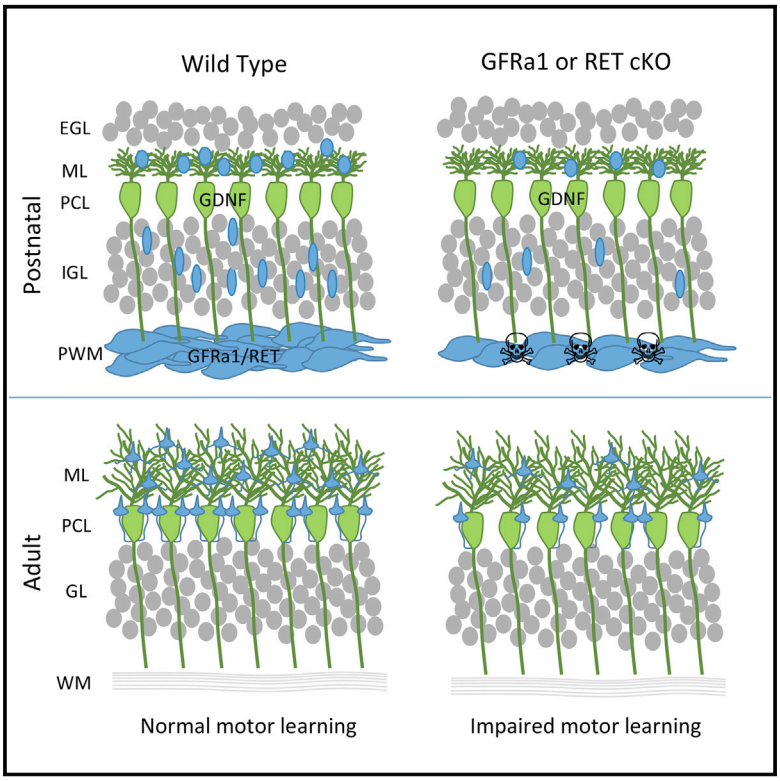

Highlights

- The signals controlling survival of molecular layer interneurons (MLIs) are unclear
- Whether MLIs are involved in normal cerebellar function was unclear
- Purkinje cells express GDNF, and survival of MLIs depends on GDNF receptors GFRα1 and RET
- Requirement of MLIs for cerebellar-dependent motor learning

Authors

Maria Christina Sergaki, Juan Carlos López-Ramos, Stefanos Stagkourakis, Agnès Gruart, Christian Broberger, José María Delgado-García, Carlos F. Ibáñez

Correspondence

carlos.ibanez@ki.se

In Brief

Sergaki et al. find that conditional mutant mice lacking GDNF receptor GFRα1 or RET lose a quarter of their cerebellar molecular layer interneurons (MLIs), resulting in compromised motor learning but not overall motor coordination. These results identify an endogenous survival mechanism for MLIs and reveal their unexpected vulnerability in the control of cerebellar-dependent motor learning

Sergaki et al., 2017, Cell Reports *19*, 1977–1986
June 6, 2017
http://dx.doi.org/10.1016/j.celrep.2017.05.030

CellPress

Cell Reports
Report

Compromised Survival of Cerebellar Molecular Layer Interneurons Lacking GDNF Receptors GFRα1 or RET Impairs Normal Cerebellar Motor Learning

Maria Christina Sergaki,[1] Juan Carlos López-Ramos,[2] Stefanos Stagkourakis,[1] Agnès Gruart,[2] Christian Broberger,[1] José María Delgado-García,[2] and Carlos F. Ibáñez[1,3,4,5,*]
[1]Department of Neuroscience, Karolinska Institute, Stockholm S-17177, Sweden
[2]Division of Neurosciences, Pablo de Olavide University, Seville 41013, Spain
[3]Department of Physiology, National University of Singapore, Singapore 117597, Singapore
[4]Life Sciences Institute, National University of Singapore, Singapore 117456, Singapore
[5]Lead Contact
*Correspondence: carlos.ibanez@ki.se
http://dx.doi.org/10.1016/j.celrep.2017.05.030

SUMMARY

The role of neurotrophic factors as endogenous survival proteins for brain neurons remains contentious. In the cerebellum, the signals controlling survival of molecular layer interneurons (MLIs) are unknown, and direct evidence for the requirement of a full complement of MLIs for normal cerebellar function and motor learning has been lacking. Here, we show that Purkinje cells (PCs), the target of MLIs, express the neurotrophic factor GDNF during MLI development and survival of MLIs depends on GDNF receptors GFRα1 and RET. Conditional mutant mice lacking either receptor lose a quarter of their MLIs, resulting in compromised synaptic inhibition of PCs, increased PC firing frequency, and abnormal acquisition of eyeblink conditioning and vestibulo-ocular reflex performance, but not overall motor activity or coordination. These results identify an endogenous survival mechanism for MLIs and reveal the unexpected vulnerability and selective requirement of MLIs in the control of cerebellar-dependent motor learning.

INTRODUCTION

The importance of the cerebellum for motor learning has long been recognized. Cerebellar circuits adjust and fine-tune motor programs to allow movement accuracy through a trial-and-error process that is critical for normal motor learning. However, the cellular and molecular components underlying these functions remain poorly characterized. Long-term depression (LTD) of the synapse between granule cell parallel fibers and Purkinje cell (PC) dendrites was initially hypothesized to be important for cerebellar motor learning (Ito, 2000), but more recent studies have indicated that motor learning can occur without cerebellar LTD (Hirano, 2014; Schonewille et al., 2011). On the other hand, the role of cerebellar molecular layer interneurons (MLIs) in shaping the computational properties of cerebellar circuits underlying plasticity and learning has lately received more attention (Jörntell et al., 2010). By performing MLI recordings on behaving animals, a recent study uncovered a positive correlation between MLI activity and classical eyeblink conditioning, a common experimental paradigm of cerebellar motor learning (ten Brinke et al., 2015). However, the direct involvement of MLIs for the expression of cerebellar motor learning responses remains to be demonstrated.

MLIs have been subdivided in basket and stellate cells according to morphological criteria. Basket cells are located in the deeper part of the molecular layer (ML) and form perineuronal nets around the perikarya of PCs that end in a brush-shaped terminal or "pinceau" on the initial segments of PC axons, which allows them to modulate PC spike output. Stellate cells are found in the superficial part of the ML, target PC dendrites, and are thought to regulate the excitatory synaptic inputs to PCs (Sotelo, 2015). Deep and superficial MLIs also show differential expression of a subset of genes that is highly enriched among cerebellar inhibitory interneurons (Schilling and Oberdick, 2009). Despite these differences, some investigators still consider stellate and basket cells as belonging to the same population (Sotelo, 2015). In the mouse cerebellum, the different GABAergic cell types are born during different time windows of development: PCs are generated first, between embryonic day (E) 10 and E12, granule layer interneurons (GLIs; i.e., Golgi cells) between E16 and postnatal day (P) 0, and MLIs within the first postnatal week (Carletti and Rossi, 2008). MLIs originate from a single progenitor pool within the cerebellar ventricular zone (VZ) that expresses the transcription factor Ptf1a (Hoshino et al., 2005). Among MLIs, basket cells are born first, around P2, and stellate cells later, around P10 (Yamanaka et al., 2004). From the VZ, MLI progenitors migrate outward to reach the prospective white matter (WM) of the embryonic cerebellum, where they persist and continue dividing for another 2 days until they turn on expression of GAD67, a key enzyme in GABA production, and resume their migration toward the ML (Cameron et al., 2009; Yamanaka et al., 2004; Zhang and Goldman, 1996). MLI migration continues within the ML for another 2–3 days until the end of the second postnatal week (Yamanaka et al., 2004). MLIs

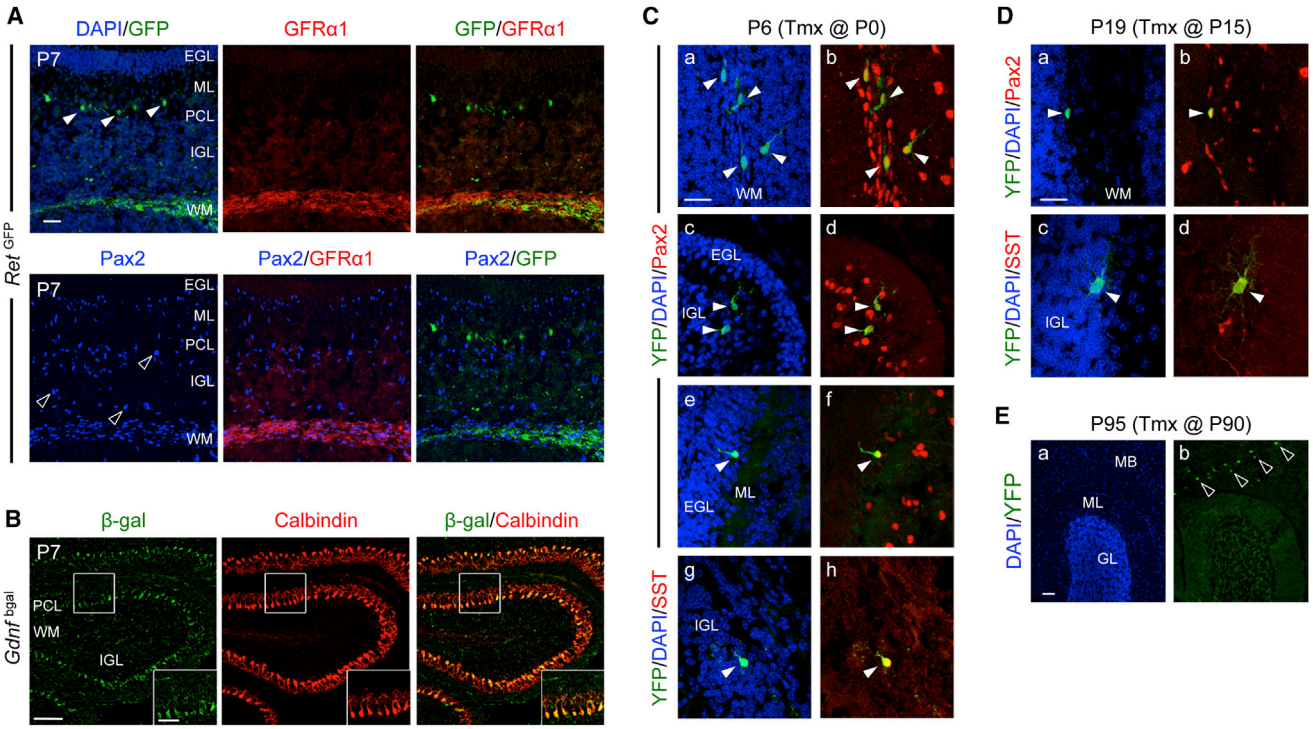

Figure 1. Expression of GFRα1, RET, and GDNF during Postnatal Cerebellar Development

(A) Sagittal cerebellar sections from P7 *Ret*^{GFP} mice stained with antibodies against GFP, GFRα1, and Pax2. Arrowheads indicate earlier born GFP^{+} MLIs (solid) and Pax2^{+} Golgi cells in the IGL (open). EGL, external granule layer; ML, molecular layer; IGL, internal granule layer; WM, white matter. The scale bar represents 100 μm.

(B) Sagittal cerebellar sections from P7 *Gdnf* ^{bgal} mice stained with β-galactosidase and calbindin antibodies. PCL, Purkinje cell layer. The scale bars represent 100 and 50 μm in bottom corner insets.

(C) Sagittal cerebellar sections from P6 *Gfra1*^{CreERT2};*R26*^{YFP} mice, injected with tamoxifen at birth (P0), stained with YFP (1–8), Pax2 (a–f), and somatostatin (SST) (g and h) antibodies and counterstained with DAPI (a, c, e, and f). Arrowheads indicate migrating MLIs (a–f) or Golgi cells (g and h). The scale bar represents 25 μm.

(D) Sagittal cerebellar sections from P19 *Gfra1*^{CreERT2};*R26*^{YFP} mice, injected with tamoxifen at P15, stained for YFP (a–d), Pax2 (a and b), and somatostatin (c and d) antibodies and counterstained with DAPI. The scale bar represents 25 μm.

(E) Sagittal cerebellar sections from P95 *Gfra1*^{CreERT2};*R26*^{YFP} mice, injected with tamoxifen at P90, stained for YFP (b), and counterstained with DAPI (a). Open arrowheads denote YFP^{+} cells in the midbrain (MB). The scale bar represents 50 μm.

undergo developmental programmed cell death, with the highest rates occurring between P5 (mainly in the WM) and P10 (as they migrate toward and within the ML) (Yamanaka et al., 2004). The signals that control MLI survival remain to be identified.

In the peripheral nervous system (PNS), neuron survival is controlled by neurotrophic factors that block developmental programmed cell death by binding and activating cognate cell surface receptors. Glial cell line-derived neurotrophic factor (GDNF) is the founding member of a small family of neurotrophic factors that regulate different processes during nervous system development, including neuron survival, cell migration, axon growth, and synapse formation (Paratcha and Ledda, 2008). GDNF receptors include an obligatory ligand binding subunit termed GDNF family receptor alpha 1 (GFRα1), which partners with one of two possible signaling subunits, the receptor tyrosine kinase RET or the neural cell adhesion molecule (NCAM), forming alternative receptor complexes (Ibáñez, 2013; Paratcha and Ledda, 2008). Despite the wealth of information available on this ligand-receptor system, its role in the development and function of the cerebellum is unknown.

In this study, we show that both GFRα1 and RET are expressed during the early stages of MLI development. Using conditional mutant mice lacking either receptor in cerebellar MLIs, we investigated the role of GFRα1/RET signaling in MLI survival and its consequences for cerebellar function and behavior.

RESULTS

Expression of GFRα1, RET, and GDNF during Postnatal Cerebellar Development

Early in situ hybridization studies indicated that *Gfra1*, *Ret*, and *Gdnf* mRNAs are expressed in the postnatal and adult rodent cerebellum (Golden et al., 1999; Trupp et al., 1997), but the precise cell types expressing the corresponding proteins remained unidentified. In order to define sites of RET and GFRα1 expression, we took advantage of the *Ret*^{GFP} mouse line that expresses GFP from the *Ret* locus and combined this with immunostaining for GFRα1 protein and the MLI progenitor marker Pax2 (Figure 1A). Although Pax2 marks the progenitors of both MLIs and GLIs, only basket and stellate cells, but not Golgi cells,

express parvalbumin (PV) when they mature. At P7, GFP and GFRα1 signals were found to colocalize with Pax2 in the prospective WM that contains MLI progenitors (Figure 1A). During development, MLI progenitors travel through the granule and PC layers to reach the ML, after which they lose Pax2 expression (Cameron et al., 2009). RET-GFP, but not GFRα1, was also found in scattered cells in the ML (Figure 1A, solid arrowheads), which likely correspond to earlier born MLIs that have already reached the ML and turned off Pax2 expression. Neither GFRα1 nor RET was found to be expressed in Pax2^{+} Golgi cells of the internal granule layer (IGL), distinguished by their larger cell bodies (Geurts et al., 2001; Weisheit et al., 2006) (Figure 1A, open arrowheads). RET-GFP expression persisted at P15 and P60 in PV^{+} MLIs located in the deeper part of the ML, where basket cells are known to reside, but was absent elsewhere in the ML, suggesting downregulation of RET expression in mature stellate cells (Figure S1A). Processes emanating from these GFP^{+} cells were seen enveloping the cell bodies of PCs, labeled with calbindin, forming characteristic perineuronal nets, a feature that distinguishes basket cells (Sotelo, 2015). No immunofluorescence signal could be detected for GFRα1 at P15 or P60 (data not shown). GDNF expression was visualized by immunohistochemistry using a *Gdnf*^{bgal} mouse line expressing beta-galactosidase from the *Gdnf* locus or by in situ hybridization. GDNF expression was found in PCs at all ages examined, from P7 to P60, and was absent in WM cells (Figures 1A, S1A, and S1C).

The presence of GFRα1 in MLI progenitors at P7 and its absence at later postnatal stages suggested transient expression of GFRα1 in cerebellar MLIs. In order to investigate this further, we used a *Gfra1*^{CreERT2} mouse line expressing tamoxifen-inducible Cre recombinase (CreERT2) from the *Gfra1* locus (Sergaki and Ibáñez, 2017). *Gfra1*^{CreERT2} mice were crossed with the *Rosa26*^{YFP} reporter line; offspring were injected with tamoxifen at P0, P15, or P90 and analyzed at P6, P19, or P95, respectively. YFP^{+} cells expressing Pax2 were found in the cerebellum of P6 and P19 mice (Figures 1C and 1D) but not at P95 (Figure 1E), indicating that GFRα1 is expressed in both early- and late-born MLI progenitors but not in mature MLIs localized at the ML. At P6, YFP^{+} cells in the ML or close to the IGL displayed morphological features of migrating MLIs, with a typical apical dendrite (Figures 1Ca–1Cf, arrowheads). Larger YFP^{+} cells expressing somatostatin (SST), a marker of Golgi neurons (Geurts et al., 2001), were also found in the IGL at P6 and P19 (Figures 1Cg and 1Ch). In summary, both RET and GFRα1 are expressed in developing MLIs of the mouse cerebellum, but, whereas RET is retained in mature basket cells, GFRα1 expression is restricted to MLI progenitors. GFRα1, but not RET, is also expressed in developing Golgi neurons, while GDNF was found in PCs at all ages.

Increased Apoptosis in MLI Progenitors Lacking GFRα1 or RET

In order to investigate the function of GFRα1 and RET in MLI progenitors, we used conditional mutants for each of the receptors. Because global knockout mice lacking either protein die at birth, we eliminated GFRα1 and RET expression by crossing *Gfra1*$^{fx/fx}$ or *Ret*$^{fx/fx}$ mice with the *Ptf1a*^{Cre} driver line. Both mutant lines (*Ptf1a*^{Cre};*Gfra1*$^{fx/fx}$ and *Ptf1a*^{Cre};*Ret*$^{fx/fx}$, respectively) survived to adulthood and had normal gross cerebellar morphology and architecture. Developmental cell death was investigated by immunostaining for activated caspase-3 at P5 in homozygous mutants and fx/fx controls lacking Cre. Increased apoptosis was observed among MLI progenitors in the folial WM in both mutant lines (Figures 2A–2D). At P10, the number of Pax2^{+} MLIs (distinguished from Golgi cells by their smaller size and morphology) was reduced in the folial WM as well as throughout the cerebellar cortex of both mutants (Figures 2E–2G and 2I–2K). On the other hand, the number of large size Pax2^{+} neurons corresponding to Golgi cells (Figures 2E and 2I, solid arrowheads) was not changed in the mutants (Figures 2H and 2L). Conditional deletion of either *Gfra1* or *Ret* with the *Gad67*^{Cre} driver, which turns on later than *Ptf1a*^{Cre}, did not affect the number of Pax2^{+} MLIs in the P10 cerebellum (Figures S2A–S2E), underscoring the requirement of GFRα1 and RET receptors for survival of MLI progenitors before they express GAD67. We also investigated whether the reduction in Pax2^{+} MLIs observed in the mutants could be due to defects in proliferation or migration. At P5, the number of proliferating cells in the folial WM, assessed 2 hr after a BrdU pulse, was not different between genotypes (Figures S3A–S3D). At this age, BrdU only marks MLI progenitors, because Golgi cells no longer proliferate. We note that some cells showing immunoreactivity for activated caspase-3 at P5 were also labeled with BrdU, indicating that both proliferating and nonproliferating cells are dying in the mutants (Figure S3E). To examine migration, we quantified the number of Pax2/BrdU double-positive cells in different layers of the cerebellar cortex at P10 (i.e., 5 days after the BrdU pulse). Again, no difference was found between genotypes (Figures S3F and S3G). Together, these data indicated that loss of GFRα1 or RET in MLI progenitors specifically compromised their survival but not proliferation or migration.

Loss of MLIs in the Cerebellum of Adult *Gfra1* and *Ret* Conditional Mutants

At 2 months of age, the cell density and overall thickness of the ML in the cerebellum of *Gfra1* and *Ret* conditional mutants was significantly reduced, as assessed by DAPI staining (Figures 3A–3C). This reduction could be accounted for by a specific loss of MLIs, as determined by the density of PV^{+} cells in this layer (Figures 3B–3E). Overall, 23% of all MLIs were missing in the cerebellum of 2-month-old *Gfra1* (23.35 ± 7.03%) and *Ret* (22.72 ± 9.06%) conditional mutants (Figures 3B and 3C). No difference was observed after deletion of *Gfra1* with the *Gad67*^{Cre} driver (Figure 3F). A smaller but significant loss of PV^{+} MLIs was also detected in 2-month-old *Gdnf* heterozygote mice (Figure 3G). To determine whether basket and stellate cells were equally affected by the loss of GFRα1, we subdivided the ML in 4 strata of equal thickness and quantified cell density in each of them. Stratum #4 is adjacent to the PC layer and thus likely contains the majority of basket cells, while the remaining strata are expected to be enriched in stellate cells. However, we found no difference in cellular distribution between *Gfra1* conditional mutants and controls (Figures S3A and S3B). In agreement with this, the density of both GFP^{+} (i.e., basket) and GFP^{-} (i.e., stellate) subpopulations of PV^{+} cells were diminished in the ML of cerebella from 2-month-old *Ptf1a*^{Cre};*Ret*$^{GFP/fx}$ mutants compared with controls (Figure 3H). Outside the cerebellum, overlap of Ptf1a

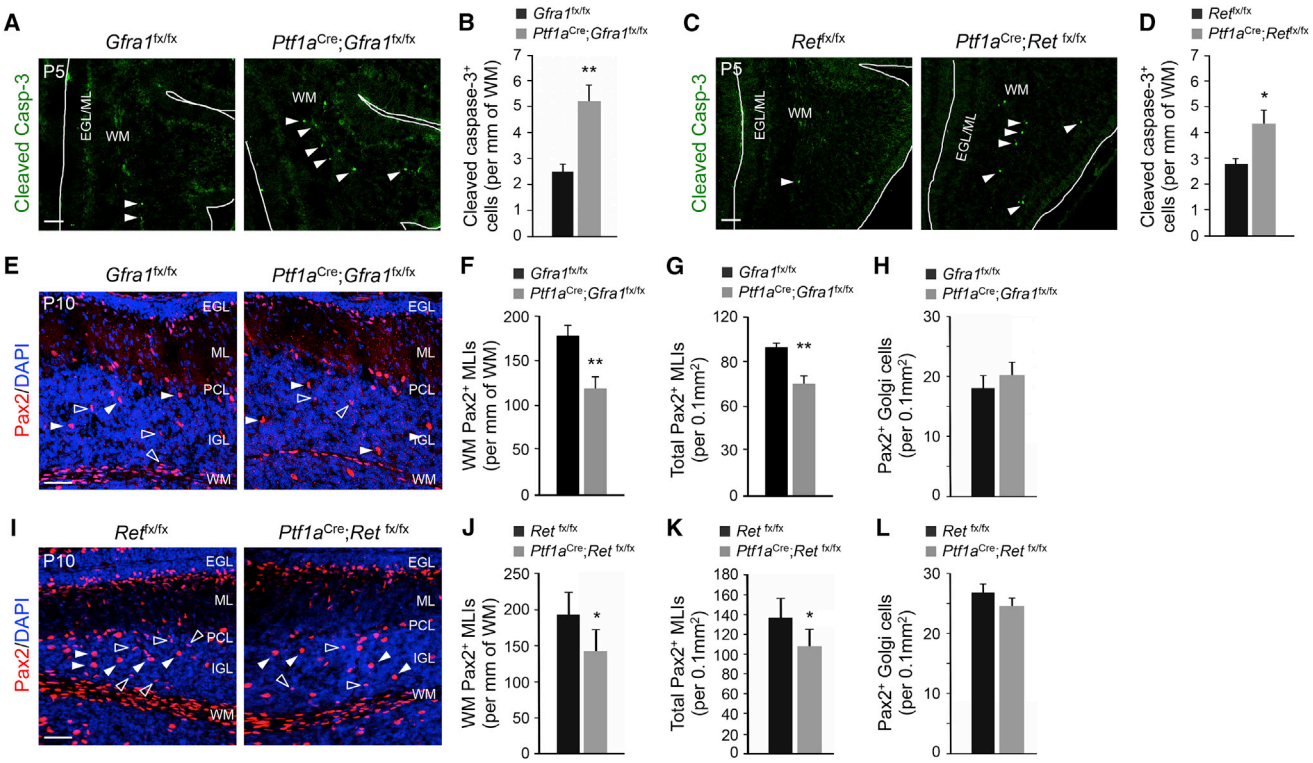

Figure 2. Increased Apoptosis in MLI Progenitors Lacking GFRα1 or RET

(A and C) Cerebellar sections from P5 *Gfra1* (A) or *Ret* (C) mutants and controls stained with cleaved-caspase-3 (Casp3) antibody. Arrows point to cleaved-Casp3$^+$ cells in the WM. White lines delineate the border of the folium. EGL, external granule layer; ML, molecular layer; WM, white matter. The scale bar represents 50 μm.

(B and D) Quantification of cleaved-Casp3$^+$ cells in the folial WM of control and *Gfra1* (B) or *Ret* (D) mutants. Values are mean ± SEM. n = 6 mice per group.

(E and I) Cerebellar sections from P10 *Gfra1* (E) or *Ret* (I) mutants and controls stained for Pax2 and counterstained with DAPI. Migratory MLIs (open arrows) and Golgi cells (solid arrows) are indicated. PCL, Purkinje cell layer; IGL, internal granule layer. The scale bar represents 50 μm.

(F, G, J, and K) Quantification of folial WM (F and J) or total (G and K) Pax2$^+$ MLI progenitor densities in P10 *Gfra1* (F and G) or *Ret* (J and K) mutants and controls. Values are mean ± SEM. n = 6 (F and G) or 5 (J and K) mice per group.

(H and L) Quantification of Pax2$^+$ Golgi cells in the IGL of P10 *Gfra1* (H) or *Ret* (L) mutants and controls. Values are mean ± SEM. n = 6 and 5 or 8 and 6 mice per group, respectively.

expression with GFRα1 could be detected only in the embryonic inferior olivary nucleus (Figure S3C). However, we did not observe any difference in the number of calbindin-expressing neurons in this area between adult controls and *Gfra1* conditional mutants (Figures S3D and S3E).

Reduced Density of Dystroglycan Puncta and Increased Firing Rate in PCs of Adult *Gfra1* and *Ret* Conditional Mutants

MLIs provide GABAergic innervation to PCs at the dendrites and the axon initial segment. Dystroglycan is a postsynaptic marker of synapses between MLIs and PC dendrites (Briatore et al., 2010). The density of dystroglycan$^+$ puncta in the ML of 2-month-old *Gfra1* conditional mutants was significantly diminished compared with *Gfra1*$^{fx/fx}$ control mice (Figures 3I and 3J), suggesting reduced GABAergic inhibition of PC dendrites. On the other hand, we saw no change in the number of pinceau terminals on the initial segment of the PC axon, as assessed by immunostaining for the specific marker Kv1.2 (Wang et al., 1993), or in the intensity of the Kv1.2 staining (Figures 3K–3M). Because axon collaterals from five to seven basket neurons contribute to the formation of each pinceau terminal (Somogyi and Hámori, 1976), a loss of 23% of MLIs would not be expected to affect the overall number of these terminals. In agreement with a reduction in GABAergic inputs on PCs, electrophysiological recordings from the somata of PCs revealed a consistent and significant increase in the firing frequency of PCs in both *Gfra1* and *Ret* mutants (Figures 3N, 3Q, S3F, and S3G), which was accompanied by decreased spontaneous inhibitory postsynaptic current (sIPSC) frequency (Figures 3O, 3R, S3H, and S3I) and rightward shift in the distribution of sIPSC inter-event intervals (Figures 3P and 3S). sIPSC amplitudes were not affected (Figures S3J and S3K). Taken together, these data demonstrated a marked impairment in PC inhibition, resulting in increased PC output in both receptor mutants due to reduced number of MLIs.

Deficient Motor Learning in Conditional Mutant Mice Lacking GFRα1 or RET in MLIs

In order to assess the behavioral consequences of the cellular and electrophysiological defects observed in the mutants, we

tested the performance of *Gfra1* and *Ret* conditional mutant mice in two paradigms that specifically evaluate cerebellum-dependent motor learning. The eyeblink is a reflex in response to corneal stimulation (Yang et al., 2015). In classical eyeblink conditioning, animals learn to associate a conditioned stimulus (CS), such as a tone, with an unconditioned stimulus (US), such as a mild electric shock to the supraorbital nerve, which evokes eyeblinks (Figure S4A). As a result of the CS-US association during training, an eyeblink conditioned response (CR) to CS presentations becomes progressively enhanced (Sánchez-Campusano et al., 2009; Thompson and Steinmetz, 2009). Figures 4A and 4C show representative electromyographic (EMG) recordings from *Gfra1* and *Ret* mutants, respectively, obtained during the seventh conditioning session (see Experimental Procedures for details). In this example, the response of the mutants to the CS was considerably diminished, although both mutant and control mice responded equally to the US in latency (e.g., 7.6 ± 0.2 ms in *Ret* mutant versus 7.5 ± 0.3 ms in control) and amplitude (0.91 ± 0.12 mV in *Ret* mutant versus 0.85 ± 0.10 mV in control). The learning curves revealed that whereas control mice acquired classical conditioning with a progressive increase in the percentage of CRs, both *Gfra1* and *Ret* mutants showed a markedly slower learning response throughout the conditioning sessions (Figures 4B and 4D).

The vestibulo-ocular reflex (VOR) helps maintain the focus on a visual image when the head turns (Figure S4B). The cerebellum plays an important role in the control of gain and phase dynamics of the VOR (Ito, 1998). VOR responses were measured in conditional *Gfra1* and *Ret* mutants at 0.1, 0.3, and 0.6 Hz (Figures 4E–4H). The mutants displayed a slower increase in VOR gain with increasing frequency (Figures 4E and 4G) and a significant increase in the number of saccades evoked by the decrease in gain (Figures 4F and 4H). Together, these results revealed significant defects in motor learning and performance of *Gfra1* and *Ret* conditional mice in two behavioral paradigms controlled by cerebellar circuits. Interestingly, no defects were observed in *Gfra1* and *Ret* conditional mutants in several other motor tests, including the open field, rotarod and balance beam tests (Figures S4D–S4G), indicating a selective impairment in motor learning rather than motor coordination or activity per se.

DISCUSSION

The prospective cerebellar WM produces different types of GABAergic interneurons at specific developmental stages from a common progenitor pool (Leto et al., 2006). The signals and molecular mechanisms that regulate this process are not well understood. Cerebellar MLIs are known to provide GABAergic innervation to PCs, but direct evidence for the necessity of a full complement of MLIs for normal cerebellar function and behavior, as well as the compensatory capacity of the MLI population, has been lacking. This study demonstrates the requirement of the GDNF/GFRα1/RET signaling pathway for the survival of cerebellar MLIs during developmental programmed cell death. Genetic disruption of this pathway resulted in the loss of approximately a quarter of cerebellar MLIs. This was sufficient to compromise synaptic inhibition of PCs and disrupt normal PC discharge and motor learning behavior. Given that no other cerebellar cell type apart from MLIs expresses RET, the effects observed in *Ret* conditional mutants are cell-autonomous to the MLIs. Although Golgi cells and PCs also transiently express GFRα1 during their early development, deletion of GFRα1 does not affect their number or distribution at postnatal stages (this study and Sergaki and Ibáñez, 2017). Given the nearly identical phenotypes of *Gfra1* and *Ret* mutants, the effects observed in *Gfra1* conditional mutants are also, in all likelihood, cell-autonomous to the MLIs.

A Full Complement of Cerebellar MLIs Is Required for Normal Cerebellum-Dependent Motor Learning but Not Motor Coordination

MLIs provide feedforward inhibition to PCs, thereby shaping PC activation in response to granule cell input (Dizon and Khodakhah, 2011). In a previous study, optogenetic activation of MLIs resulted in a brief suppression of spontaneous PC firing, which was sufficient to cause small orofacial movements in mice (Heiney et al., 2014). Although this result indicated a link between MLI function and movement generation, it did not provide evidence for a role of MLIs in motor learning. Moreover, as this was based on a gain-of-function strategy, the requirement of MLIs was not established in those experiments. Other studies reported that genetic ablation of the γ2 subunit of the GABA-A receptor in PCs resulted in irregular spike firing and impaired ability to adapt the phase of the VOR (Wulff et al., 2009), as well as defects in conditioned eyeblink responses (ten Brinke et al., 2015), indirectly implicating MLI-mediated inhibition in those functions. However, GABA-B receptor-mediated inhibition of PCs was unchanged in those mice (Wulff et al., 2009), and deletion of synaptic GABA-A receptors in PCs would also have disrupted any inhibition mediated by recurrent collaterals of PC axons. By compromising the survival mechanisms of MLIs, our study is the first to provide direct evidence for the requirement of these neurons for normal PC activity and cerebellar-dependent motor learning. At the circuit level, our analysis of synaptic contacts between MLIs and PCs revealed a reduction in GABAergic inputs to PC dendrites but not in pinceau terminals on the axon initial segment in *Gfra1* mutant mice. This suggests that a decrease in dendritic GABAergic input may be sufficient to affect PC firing frequency. *Gfra1* and *Ret* conditional mutants performed significantly worse than control mice in both the eyeblink conditioning and VOR paradigms, showing slower learning acquisition and failure to adjust gain responses. However, these mice performed normally in the rotarod and balance beam tests, two classical assays of cerebellum-dependent motor coordination. This indicates a selective impairment in motor learning, rather than motor coordination or activity per se, caused by a partial loss of cerebellar MLIs, and suggests distinct underlying circuitry controlling motor learning and activity. The fact that mutant mice still retained more than 75% of cerebellar MLIs underscores the importance of a full complement of cerebellar MLIs for normal cerebellum-dependent motor learning, as loss of only a quarter of all cerebellar MLIs was sufficient to cause abnormalities. In contrast, for example, the basal ganglia can withstand the loss of more than two-thirds of nigral dopaminergic neurons before Parkinsonian symptoms emerge (Dauer and Przedborski, 2003). Our results therefore

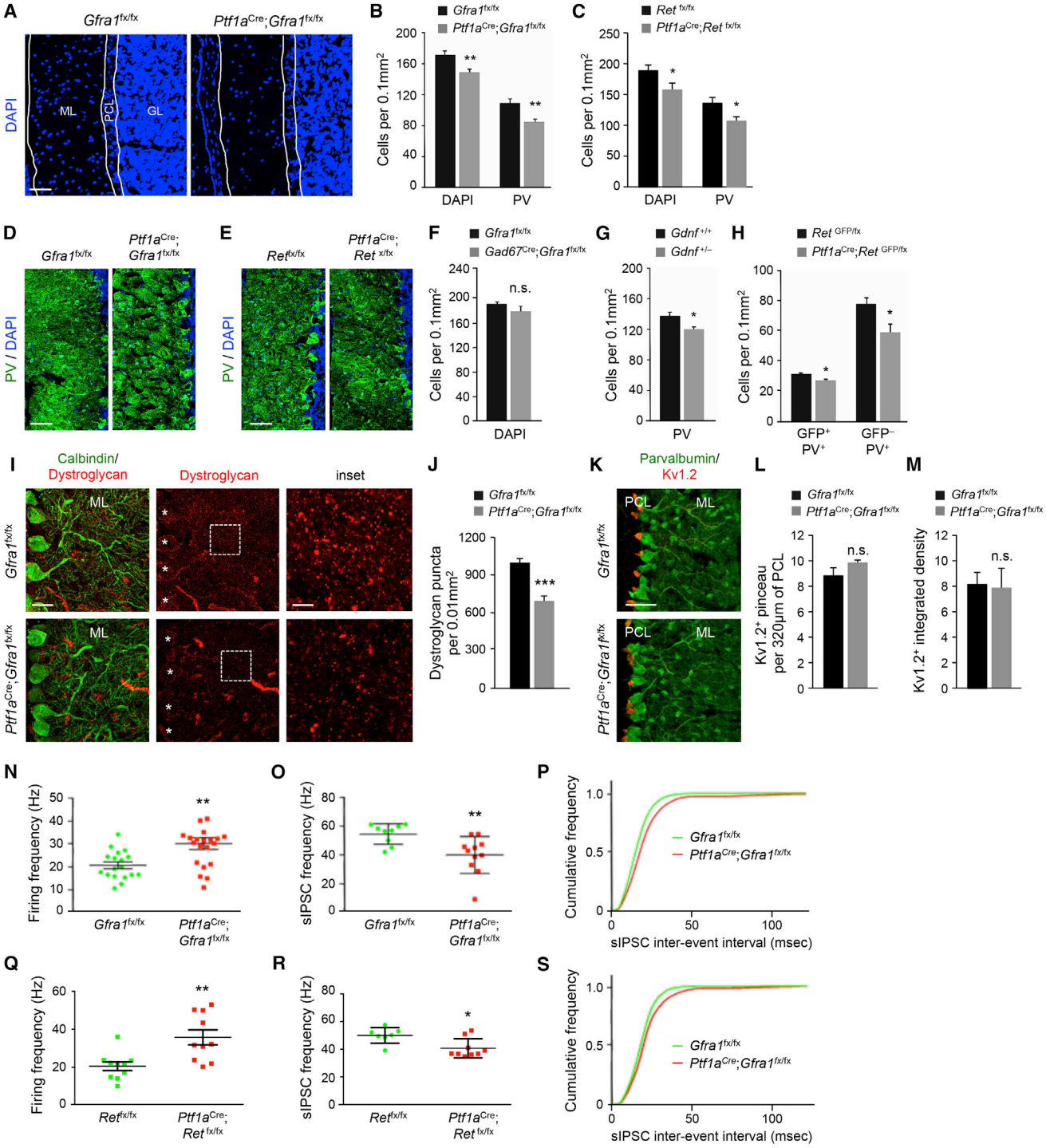

Figure 3. Loss of MLInterneurons Reduced GABAergic Synapses and Increased PC Firing Rate in the Cerebellum of Adult *Gfra1* and *Ret* Conditional Mutants

(A) Cerebellar sections from 2-month-old *Gfra1* mutants and controls stained with DAPI. White lines denote cerebellar layers (as identified from PV staining, not shown here). ML, molecular layer; PCL, Purkinje cell layer; GL, granule layer. The scale bar represents 50 µm.

(B and C) Quantification of $DAPI^+$ and PV^+ cells in the ML of 2-month-old *Gfra1* (B) or *Ret* (C) mutants and controls. Values are mean ± SEM. n = 6 (B) or 5 (C) mice per group, respectively.

(D and E) Cerebellar sections from 2-month-old *Gfra1* (D) or *Ret* (E) mutants and controls stained with parvalbumin (PV) and counterstained with DAPI. The scale bar represents 50 µm.

(legend continued on next page)

reveal an unexpected vulnerability to the loss of even a minority of the MLI population.

MLIs Depend on GDNF/GFRα1/RET Signaling for Survival during Developmental Programmed Cell Death

Cerebellar MLIs undergo developmental programmed cell death between P5 and P10 (Yamanaka et al., 2004) but the mechanisms that control this process have been unknown. Unlike the situation in the PNS, the role of neurotrophic factors in the control of programmed cell death in the brain remains controversial. Although GDNF was initially discovered for its ability to promote survival of midbrain dopaminergic neurons in vitro and upon injury, mice lacking RET in dopaminergic neurons show either no defects (Jain et al., 2006) or only a marginal neuronal loss at very advanced age (Kramer et al., 2007). A report that initially claimed the absolute requirement of GDNF for survival of brain catecholaminergic neurons (Pascual et al., 2008) has more recently been challenged (Kopra et al., 2015). To date, most of the neurotrophic factors that promote survival of PNS neurons have not shown similar effects in developing neurons of the brain. This has led to the idea that other stimuli, such as neuronal activity and neurotransmitter input, play a more important role in regulating neuronal survival in the brain (Dekkers et al., 2013). The results of the present study show that signaling by GFRα1 and RET is required for the survival of cerebellar MLIs during their period of developmental programmed cell death. GDNF was expressed during the same time window by PCs (i.e., the target of MLIs). As PC axons travel through the WM to reach neurons in the deep nuclei, MLI progenitors may obtain GDNF from these axons. Together with the loss of a fraction of MLIs in *Gdnf* heterozygote mutant mice, these data suggest that a target-derived neurotrophic circuit operates to control the survival of this neuronal population during development. Although all MLI progenitors were seen to express GFRα1 and RET, only about a quarter of all MLIs were lost in *Gfra1* and *Ret* mutants, suggesting heterogeneous survival requirements in these cells. The fact that MLIs were lost in equal proportion in all ML strata as well as among basket and stellate cells, argues against the loss of a particular MLI subtype in the mutants.

Conclusions

This study demonstrates the dependence of cerebellar MLIs on PC-derived GDNF for their survival during developmental programmed cell death and provides direct evidence for the requirement of a full complement of MLIs for cerebellum-dependent motor learning. The unexpected vulnerability to the loss of a fraction of MLIs reveals a previously unappreciated lack of redundancy in the cerebellar circuitry that controls motor learning.

EXPERIMENTAL PROCEDURES

For detailed procedures, see Supplemental Experimental Procedures.

Ethics Statement

All animal experiments were approved by Stockholm North Ethical Committee for Animal Research (protocols N27/15, N173/15, and N26/15).

Statistical Analysis

For image analysis, Student's t test was used for evaluation of the statistical significance of the results. For slice recordings, the two-sample Kolmogorov-Smirnov (K-S2) test was used to compare pooled cumulative frequency distributions. For behavioral studies, statistical analyses were carried out using the SPSS package (SPSS) for a statistical significance level of $p < 0.05$.

Histological Studies

For immunostaining, cerebellar sections were blocked for 1 hr in PBS containing 5% normal donkey serum and 0.1% Triton X-100. Incubation with primary antibodies, diluted in blocking solution, was done overnight (o/n) at 4°C. Sections were washed 3 × 10 min in PBS and then incubated with fluorescently labeled secondary antibodies (diluted in blocking solution) and 1 μg/mL DAPI (D1306; Sigma) for counterstaining for 2 hr at room temperature (RT). The slides were finally washed 3 × 10 min in PBS and mounted with DAKO fluorescent medium.

Genetic Fate Mapping and BrdU Labeling

For genetic fate mapping, *Gfra1*^{CreERT2};*Rosa26*^{YFP} mice received a single subcutaneous injection of 2 mg/30 g tamoxifen (Tmx; Sigma) dissolved in corn oil (Sigma) containing 10% ethanol at P0, P15, and P90.

For BrdU labeling, pups were injected subcutaneously with 25 mg/kg BrdU (Sigma) in PBS at P5. Embryos were collected 2 hr after injection for proliferation analysis or 5 days later for migration studies. For BrdU detection, sections were incubated in 2 N HCl, 0.1% Triton X-100 at 37°C for 20 min, washed with 0.1 M sodium borate for 15 min, washed 2 × 5 min with PBS, and incubated with rat anti-BrdU antibody.

Image Analysis

All fluorescent images were captured with a Carl Zeiss LSM710 confocal microscope using ZEN 2009 software (Carl Zeiss), and cell counts were made with ImageJ software (http://imagej.nih.gov/ij/). For caspase-3 analysis, counts were made in the entire length of folial WM from six sagittal sections (14 μm thick, one section every 140 μm) per animal from medial to lateral planes. For Pax2 MLI and Golgi cell counts, two images, containing all layers

(F) Quantification of DAPI$^+$ cells in the ML of 2-month-old *Gad67*^{Cre};*Gfra1*$^{fx/fx}$ mutants and controls. Values are mean ± SEM. n = 3 mice per group.
(G) Quantification of PV$^+$ cells in the ML of 2-month-old wild-type and heterozygous *Gdnf* mutant mice. Values are mean ± SEM. n = 6 mice per group.
(H) Quantification of GFP$^+$/PV$^+$ double-positive and GFP$^-$/PV$^+$ cells in the ML of 2-month-old *Ret* mutants and controls. Values are mean ± SEM. n = 6 and 8 mice per group, respectively.
(I) Cerebellar sections from 2-month-old *Gfra1* mutants and controls stained with calbindin and dystroglycan antibodies. Asterisk denotes cell bodies of PCs. The scale bars represent 25 μm (left) and 5 μm (insets).
(J) Quantification of dystroglycan$^+$ puncta in the ML of 2-month-old *Gfra1* mutants and controls. Values represent mean ± SEM. n = 6 and 7 mice per group, respectively.
(K) Cerebellar sections from 2-month-old *Gfra1* mutants and controls stained with Kv1.2 and calbindin antibodies as indicated. The scale bar represents 50 μm.
(L and M) Quantification of the number of Kv1.2$^+$ pinceau synapses (L) and Kv1.2 staining intensity (M) in the PCL of 2 month old *Gfra1* mutants and controls. Values are mean ± SEM. n = 3 mice per group, respectively. n.s., not significantly different ($p > 0.05$).
(N and Q) PC firing frequency in cerebella of 2-month-old *Gfra1* (N) or *Ret* (Q) mutants and controls. Each dot denotes mean from 300 s recording from individual PC. Mean and SEM are shown with parallel lines. n = 18 and 20 (N) or 5 and 7 (Q) PCs per group, respectively.
(O and R) sIPSC frequency in PCs from *Gfra1* (O) or *Ret* (R) mutants and controls. n = 9 and 11 or 6 and 5 PCs per group, respectively.
(P and S) Cumulative frequency diagram of sIPSC inter-event interval in PCs from *Gfra1* (P) or *Ret* (S) mutants and controls (Kolmogorov-Smirnov, $p < 0.0001$).

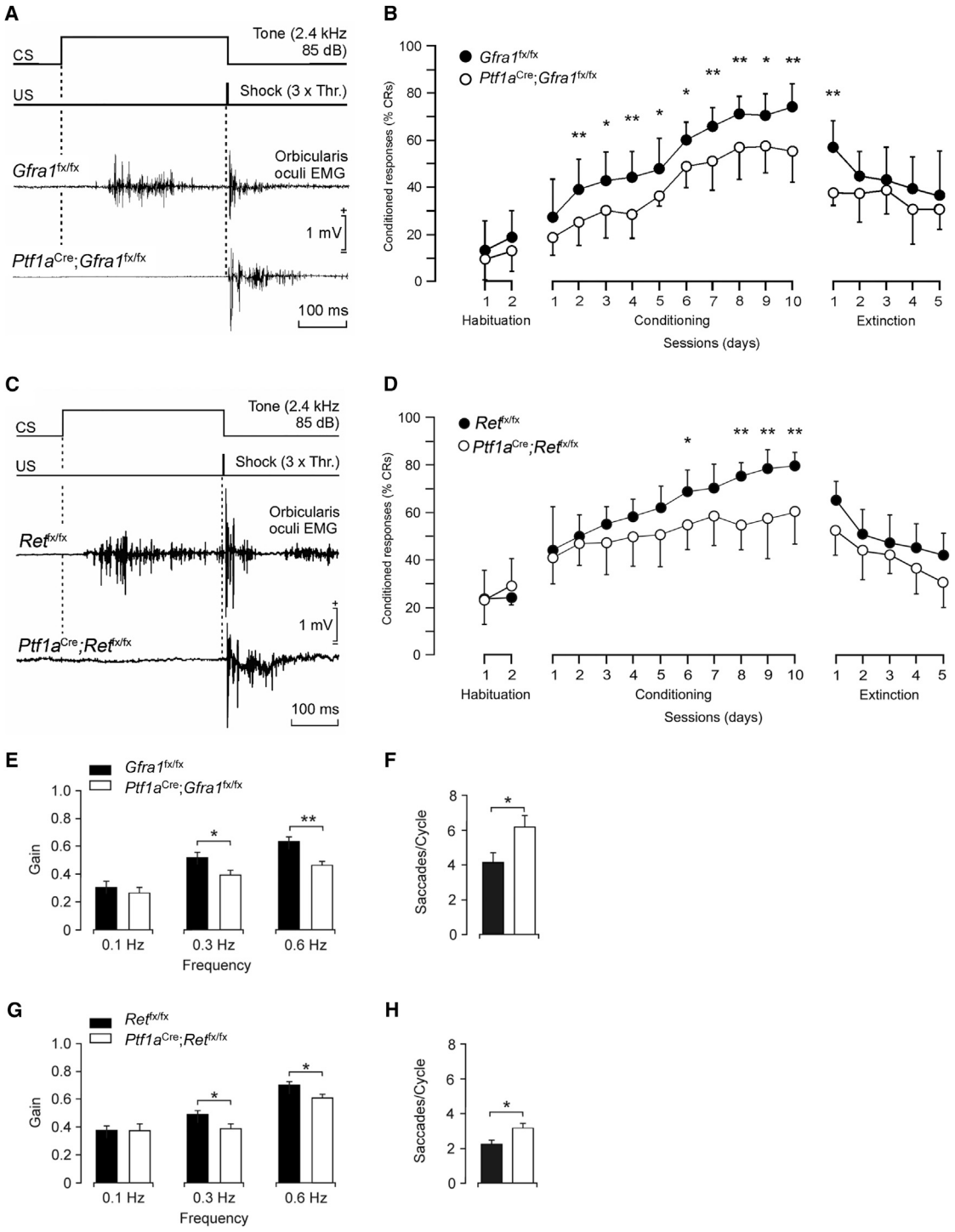

Figure 4. Deficient Motor Learning in Adult *Gfra1* and *Ret* Conditional Mutants

(A and C) EMG recordings from the Obicularis oculi (O.O.) muscle obtained in 2-month-old *Gfra1* (A) and *Ret* (C) mutants and controls during the seventh conditioning session. Schematics of conditioned stimulus (CS) and unconditioned stimulus (US) are shown at the top.

(B and D) Percentage of conditioned responses (CRs) during habituation, conditioning, and extinction sessions in 2-month-old *Gfra1* (B) and *Ret* (D) mutants and their respective controls. Values are mean ± SEM. n = 8 mice per group.

(E and G) Bode plots for gain VOR reflexes recorded in a lighted room from *Gfra1* (E) and *Ret* (G) mutants and their respective controls. Values are mean ± SEM. n = 8 mice per group. *p < 0.05 (two-way ANOVA).

(F and H) Mean number of compensatory saccades per cycle carried out by *Gfra1* (F) and *Ret* (H) mutants and their respective controls. *p < 0.05, **p < 0.01 (two-way ANOVA).

of the cerebellar cortex, were obtained from each folium, approximately at the same location, and two midsagittal sections (14 μm) were analyzed per mouse. For counts in adult tissue, $DAPI^+$, PV^+ cells or $dystroglycan^+$ puncta were analyzed in the ML and $Kv1.2^+$ synapses on PC cell bodies.

Cerebellar Slice Recordings

Whole-cell recordings were made from PC somata primarily located in lobules 4–7 (Larsell, 1952) at near physiological temperature (34°C). The holding potential in voltage-clamp recordings was 60 mV. Recordings of sIPSCs were performed in voltage-clamp mode in the presence of 10 μM CNQX and 25 μM AP-5 to block ionotropic glutamatergic neurotransmission. All sIPSCs recordings were concluded by application of 10 μM gabazine to confirm the GABAergic nature of events by the complete loss of all synaptic currents. Recordings were performed using a Multiclamp 700B amplifier, a DigiData 1440, and pClamp10.2 software (Molecular Devices).

Behavioral Studies

Classical conditioning was achieved using a delay paradigm. The US consisted of a cathodal, square pulse applied to the supraorbital nerve (500 μs, 3 × threshold) at the end of the CS. A total of 2 habituation, 10 conditioning, and 5 extinction sessions were carried out for each animal. A conditioning session consisted of 60 CS-US presentations and lasted 30 min. For vestibular stimulation, a single animal was placed on a homemade turning-table system. Eye positions for each frequency and animal were averaged (10 complete rotations × 3 recording sessions) for offline analysis of gain and phase (de Jeu and De Zeeuw, 2012). The number of compensatory eye saccades was also quantified.

SUPPLEMENTAL INFORMATION

Supplemental Information includes Supplemental Experimental Procedures and four figures and can be found with this article online at http://dx.doi.org/10.1016/j.celrep.2017.05.030.

AUTHOR CONTRIBUTIONS

M.C.S. designed and performed all experiments (except electrophysiological studies, VOR, and eyeblink conditioning) and prepared the first draft of the manuscript and figures. J.C.L.-R., A.G., and J.M.D.-G. performed the VOR and eyeblink conditioning experiments. S.S. and C.B. performed the electrophysiological studies. C.F.I. contributed to the design of experiments and interpretation of results and produced the final version of the manuscript and figures.

ACKNOWLEDGMENTS

We thank Diana Fernández Suárez for help with calbindin staining of adult brainstem sections; Francoise Helmbacher (IBDML, Marseille, France) for providing brain tissue from *Gdnf*^{hgal} mice; Mart Saarma and Jaan-Olle Andressoo (University of Helsinki, Finland) for *Gfra1*$^{fx/fx}$ mice; and Annika Andersson, José A. Santos-Naharro, and José M. González-Martín for technical assistance. Support was provided by grants from the Swedish Research Council (2016-01538), the Knut and Alice Wallenbergs Foundation (Wallenberg Scholars Program; KAW 2012.0270), and the National University of Singapore (R-185-000-227-133 and -733 to C.F.I.); from MINECO (BFU21014-56692-R to A.G. and J.M.D.-G.); and from the European Research Council (ENDOSWITCH 261286) and the Swedish Research Council (to C.B.).

Received: February 5, 2017
Revised: March 29, 2017
Accepted: May 9, 2017
Published: June 6, 2017

REFERENCES

Briatore, F., Patrizi, A., Viltono, L., Sassoè-Pognetto, M., and Wulff, P. (2010). Quantitative organization of GABAergic synapses in the molecular layer of the mouse cerebellar cortex. PLoS ONE *5*, e12119.

Cameron, D.B., Kasai, K., Jiang, Y., Hu, T., Saeki, Y., and Komuro, H. (2009). Four distinct phases of basket/stellate cell migration after entering their final destination (the molecular layer) in the developing cerebellum. Dev. Biol. *332*, 309–324.

Carletti, B., and Rossi, F. (2008). Neurogenesis in the cerebellum. Neuroscientist *14*, 91–100.

Dauer, W., and Przedborski, S. (2003). Parkinson's disease: mechanisms and models. Neuron *39*, 889–909.

de Jeu, M., and De Zeeuw, C.I. (2012). Video-oculography in mice. J. Vis. Exp. *65*, e3971.

Dekkers, M.P.J., Nikoletopoulou, V., and Barde, Y.-A. (2013). Cell biology in neuroscience: Death of developing neurons: new insights and implications for connectivity. J. Cell Biol. *203*, 385–393.

Dizon, M.J., and Khodakhah, K. (2011). The role of interneurons in shaping Purkinje cell responses in the cerebellar cortex. J. Neurosci. *31*, 10463–10473.

Geurts, F.J., Timmermans, J., Shigemoto, R., and De Schutter, E. (2001). Morphological and neurochemical differentiation of large granular layer interneurons in the adult rat cerebellum. Neuroscience *104*, 499–512.

Golden, J.P., DeMaro, J.A., Osborne, P.A., Milbrandt, J., and Johnson, E.M., Jr. (1999). Expression of neurturin, GDNF, and GDNF family-receptor mRNA in the developing and mature mouse. Exp. Neurol. *158*, 504–528.

Heiney, S.A., Kim, J., Augustine, G.J., and Medina, J.F. (2014). Precise control of movement kinematics by optogenetic inhibition of Purkinje cell activity. J. Neurosci. *34*, 2321–2330.

Hirano, T. (2014). Around LTD hypothesis in motor learning. Cerebellum *13*, 645–650.

Hoshino, M., Nakamura, S., Mori, K., Kawauchi, T., Terao, M., Nishimura, Y.V., Fukuda, A., Fuse, T., Matsuo, N., Sone, M., et al. (2005). Ptf1a, a bHLH transcriptional gene, defines GABAergic neuronal fates in cerebellum. Neuron *47*, 201–213.

Ibáñez, C.F. (2013). Structure and physiology of the RET receptor tyrosine kinase. Cold Spring Harb. Perspect. Biol. *5*, 1–10.

Ito, M. (1998). Cerebellar learning in the vestibulo-ocular reflex. Trends Cogn. Sci. *2*, 313–321.

Ito, M. (2000). Mechanisms of motor learning in the cerebellum. Brain Res. *886*, 237–245.

Jain, S., Golden, J.P., Wozniak, D., Pehek, E., Johnson, E.M., Jr., and Milbrandt, J. (2006). RET is dispensable for maintenance of midbrain dopaminergic neurons in adult mice. J. Neurosci. *26*, 11230–11238.

Jörntell, H., Bengtsson, F., Schonewille, M., and De Zeeuw, C.I. (2010). Cerebellar molecular layer interneurons - computational properties and roles in learning. Trends Neurosci. *33*, 524–532.

Kopra, J., Vilenius, C., Grealish, S., Härma, M.-A., Varendi, K., Lindholm, J., Castrén, E., Võikar, V., Björklund, A., Piepponen, T.P., et al. (2015). GDNF is not required for catecholaminergic neuron survival in vivo. Nat. Neurosci. *18*, 319–322.

Kramer, E.R., Aron, L., Ramakers, G.M., Seitz, S., Zhuang, X., Beyer, K., Smidt, M.P., and Klein, R. (2007). Absence of Ret signaling in mice causes progressive and late degeneration of the nigrostriatal system. PLoS Biol. *5*, e39.

Larsell, O. (1952). The morphogenesis and adult pattern of the lobules and fissures of the cerebellum of the white rat. J. Comp. Neurol. *97*, 281–356.

Leto, K., Carletti, B., Williams, I.M., Magrassi, L., and Rossi, F. (2006). Different types of cerebellar GABAergic interneurons originate from a common pool of multipotent progenitor cells. J. Neurosci. *26*, 11682–11694.

Paratcha, G., and Ledda, F. (2008). GDNF and GFRalpha: a versatile molecular complex for developing neurons. Trends Neurosci. *31*, 384–391.

Pascual, A., Hidalgo-Figueroa, M., Piruat, J.I., Pintado, C.O., Gómez-Díaz, R., and López-Barneo, J. (2008). Absolute requirement of GDNF for adult catecholaminergic neuron survival. Nat. Neurosci. *11*, 755–761.

Sánchez-Campusano, R., Gruart, A., and Delgado-García, J.M. (2009). Dynamic associations in the cerebellar-motoneuron network during motor learning. J. Neurosci. *29*, 10750–10763.

Schilling, K., and Oberdick, J. (2009). The treasury of the commons: making use of public gene expression resources to better characterize the molecular diversity of inhibitory interneurons in the cerebellar cortex. Cerebellum *8*, 477–489.

Schonewille, M., Gao, Z., Boele, H.-J., Veloz, M.F., Amerika, W.E., Šimek, A.A.M., De Jeu, M.T., Steinberg, J.P., Takamiya, K., Hoebeek, F.E., et al. (2011). Reevaluating the role of LTD in cerebellar motor learning. Neuron *70*, 43–50.

Sergaki, M.C., and Ibáñez, C.F. (2017). GFRα1 regulates Purkinje cell migration by counteracting NCAM function. Cell Rep. *18*, 367–379.

Somogyi, P., and Hámori, J. (1976). A quantitative electron microscopic study of the Purkinje cell axon initial segment. Neuroscience *1*, 361–365.

Sotelo, C. (2015). Molecular layer interneurons of the cerebellum: developmental and morphological aspects. Cerebellum *14*, 534–556.

ten Brinke, M.M., Boele, H.-J., Spanke, J.K., Potters, J.-W., Kornysheva, K., Wulff, P., IJpelaar, A.C.H.G., Koekkoek, S.K.E., and De Zeeuw, C.I. (2015). Evolving models of Pavlovian conditioning: cerebellar cortical dynamics in awake behaving mice. Cell Rep. *13*, 1977–1988.

Thompson, R.F., and Steinmetz, J.E. (2009). The role of the cerebellum in classical conditioning of discrete behavioral responses. Neuroscience *162*, 732–755.

Trupp, M., Belluardo, N., Funakoshi, H., and Ibáñez, C.F. (1997). Complementary and overlapping expression of glial cell line-derived neurotrophic factor (GDNF), c-ret proto-oncogene, and GDNF receptor-alpha indicates multiple mechanisms of trophic actions in the adult rat CNS. J. Neurosci. *17*, 3554–3567.

Wang, H., Kunkel, D.D., Martin, T.M., Schwartzkroin, P.A., and Tempel, B.L. (1993). Heteromultimeric K+ channels in terminal and juxtaparanodal regions of neurons. Nature *365*, 75–79.

Weisheit, G., Gliem, M., Endl, E., Pfeffer, P.L., Busslinger, M., and Schilling, K. (2006). Postnatal development of the murine cerebellar cortex: formation and early dispersal of basket, stellate and Golgi neurons. Eur. J. Neurosci. *24*, 466–478.

Wulff, P., Schonewille, M., Renzi, M., Viltono, L., Sassoè-Pognetto, M., Badura, A., Gao, Z., Hoebeek, F.E., van Dorp, S., Wisden, W., et al. (2009). Synaptic inhibition of Purkinje cells mediates consolidation of vestibulo-cerebellar motor learning. Nat. Neurosci. *12*, 1042–1049.

Yamanaka, H., Yanagawa, Y., and Obata, K. (2004). Development of stellate and basket cells and their apoptosis in mouse cerebellar cortex. Neurosci. Res. *50*, 13–22.

Yang, Y., Lei, C., Feng, H., and Sui, J.-F. (2015). The neural circuitry and molecular mechanisms underlying delay and trace eyeblink conditioning in mice. Behav. Brain Res. *278*, 307–314.

Zhang, L., and Goldman, J.E. (1996). Developmental fates and migratory pathways of dividing progenitors in the postnatal rat cerebellum. J. Comp. Neurol. *370*, 536–550.

Cell Reports, Volume *19*

Supplemental Information

Compromised Survival of Cerebellar Molecular Layer Interneurons Lacking GDNF Receptors GFRα1 or RET Impairs Normal Cerebellar Motor Learning

Maria Christina Sergaki, Juan Carlos López-Ramos, Stefanos Stagkourakis, Agnès Gruart, Christian Broberger, José María Delgado-García, and Carlos F. Ibáñez

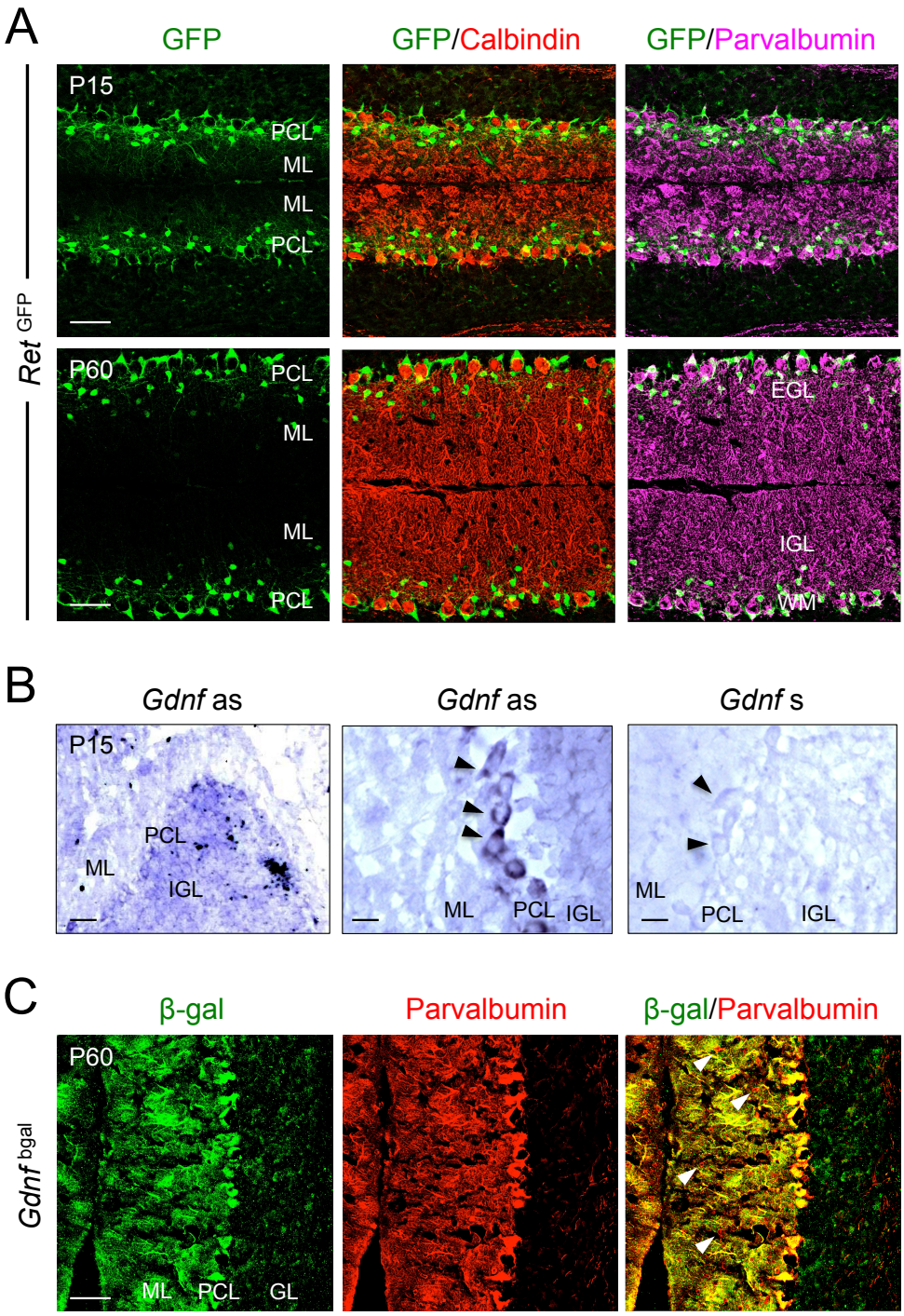

Supplementary Figure S1. Related to Fig. 1. Expression of RET and GDNF during postnatal cerebellar development

(A) Sagittal cerebellar sections from P15 and P60 *Ret*^{GFP} mice immunostained for GFP (green), Calbindin (red) and Parvalbumin (purple). GFP was localized to the inner part of the molecular layer. GFP$^+$ axons were seen enveloping Calbindin$^+$ PC bodies, a characteristic of basket cells. GFP$^+$ signal co-localized with Parvalbumin in MLIs but not in PCs, which also express PV. PCL: Purkinje cell layer, ML: molecular layer. Scale bar, 50μm.

(B) Sagittal cerebellar sections from P15 wild type mice hybridized with *Gdnf* antisense (as) and sense (s) riboprobes. Arrowheads point to PCs strongly expressing the *Gdnf* mRNA in sections incubated with the antisense probe. Lower intensity signal was detected in the IGL. No signal was detected in the ML or in sections incubated with the sense probe. ML: molecular layer, PCL: Purkinje cell layer, IGL: internal granule layer. Scale bar, 500μm (far left) and 100 μm (center and far right).

(C) Sagittal cerebellar sections from P60 *Gdnf*^{bgal} mice immunostained for β-galactosidase and Parvalbumin (PV). GDNF expression was mainly found in PCs (labeled here with anti-PV antibodies), with lower levels present in the granule layer (GL). No GDNF expression was observed in PV$^+$ MLIs (arrowheads). ML: molecular layer, PCL: Purkinje cell layer, GL: granule layer. Scale bar, 50μm.

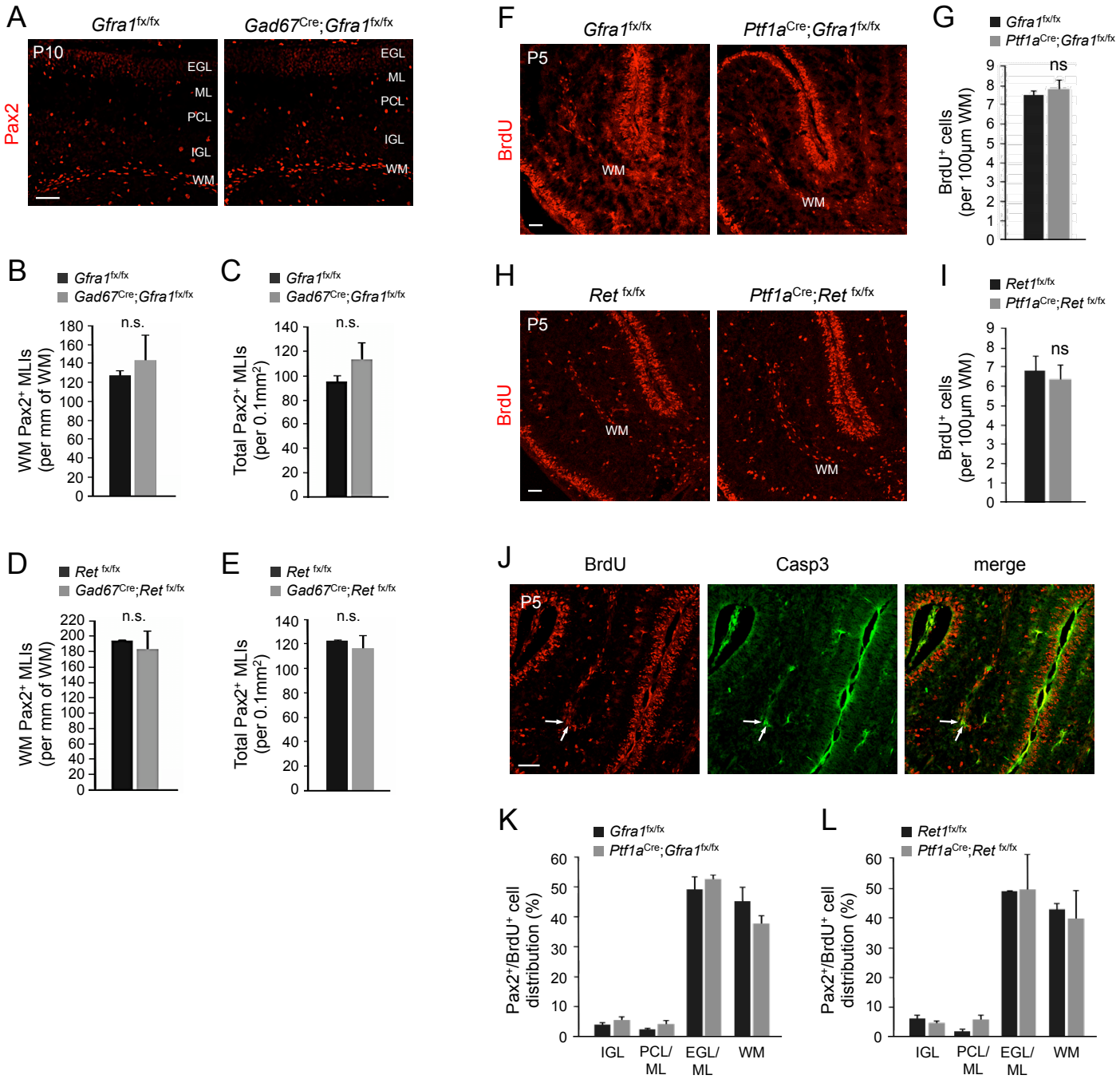

Supplementary Figure S2. Related to Fig. 2. No effect of deletion of *Gfra1* or *Ret* with *Gad67*^{CRE} in cerebellum and normal proliferation and migration of MLI progenitors in *Gfra1* and *Ret* conditional mutants

(A) Cerebellar sections from P10 *Gad67*^{Cre};*Gfra1*$^{fx/fx}$ conditional mutant mice and *Gfra1*$^{fx/fx}$ controls stained with Pax2 antibodies. EGL: external granule layer, ML: molecular layer, PCL: Purkinje cell layer, IGL: internal granule layer, WM: white matter. Scale bar, 50µm.

(B) Quantification of Pax2$^+$ progenitor density in the folial WM of P10 *Gad67*^{Cre};*Gfra1*$^{fx/fx}$ conditional mutant mice and *Gfra1*$^{fx/fx}$ controls. Values represent mean ±SEM. N=3 mice per group. n.s; not significantly different.

(C) Quantification of the total Pax2$^+$ MLI progenitor density in the cerebellar cortex of P10 *Gad67*^{Cre};*Gfra1*$^{fx/fx}$ conditional mutant mice and *Gfra1*$^{fx/fx}$ controls. Values represent mean ±SEM. N=3 mice per group. n.s; not significantly different.

(D) Quantification of Pax2$^+$ progenitors in the folial WM of P10 *Gad67*^{Cre};*Ret*$^{fx/fx}$ conditional mutant mice and *Ret*$^{fx/fx}$ controls. Values represent mean ±SEM. N=3 mice per group. n.s; not significantly different.

(E) Quantification of the total Pax2$^+$ MLI progenitor density in the cerebellar cortex of P10 *Gad67*^{Cre};*Ret*$^{fx/fx}$ conditional mutant mice and *Ret*$^{fx/fx}$ controls. Values represent mean ±SEM. N=3 mice per group. n.s; not significantly different.

(F) Cerebellar sections from P5 *Gfra1* conditional mutant mice (*Ptf1a*^{Cre};*Gfra1*$^{fx/fx}$) and controls (*Gfra1*$^{fx/fx}$) stained with BrdU antibodies 2h after a BrdU pulse. WM: white matter. Scale bar, 50µm.

(G) Quantification of BrdU$^+$ cells in WM of conditional *Gfra1* mutant mice and controls. Values represent mean ±SEM. N=6 and 4 mice per group, respectively. n.s; not significantly different.

(H) Cerebellar sections from P5 *Ret* conditional mutant mice (*Ptf1a*^{Cre};*Ret*$^{fx/fx}$) and controls (*Ret*$^{fx/fx}$) stained with BrdU antibodies 2h after a BrdU pulse. WM: white matter. Scale bar, 50µm.

(I) Quantification of BrdU$^+$ cells in WM of conditional *Ret* mutant mice and controls. Values represent mean ±SEM. N=5 and 6 mice per group, respectively. n.s; not significantly different.

(J) Activated caspase-3 and BrdU in WM of conditional *Gfra1* mutant mice. Arrows indicate cells that incorporated BrdU and show activation of caspase-3. Scale bar 50µm.

(K) Quantification of the percentage of Pax2$^+$/BrdU$^+$ double-positive cells in each layer of the cerebellar cortex relative to the total number of double-labeled cells in *Gfra1* conditional mutant mice (*Ptf1a*^{Cre};*Gfra1*$^{fx/fx}$) and controls (*Gfra1*$^{fx/fx}$) injected with BrdU at P5 and sacrificed at P10. EGL: external granule layer, ML: molecular layer, PCL: Purkinje cell layer, IGL: internal granule layer, WM: white matter. Values represent mean ±SEM. N=5 and 4 mice per group, respectively. n.s: not significantly different.

(L) Quantification of the percentage of Pax2$^+$/BrdU$^+$ double-positive cells in each layer of the cerebellar cortex relative to the total number of double-labeled cells in *Ret* conditional mutant mice (*Ptf1a*^{Cre};*Ret*$^{fx/fx}$) and controls (*Ret*$^{fx/fx}$) injected with BrdU at P5 and sacrificed at P10. Values represent mean ±SEM. N=3 mice per group. n.s: not significantly different.

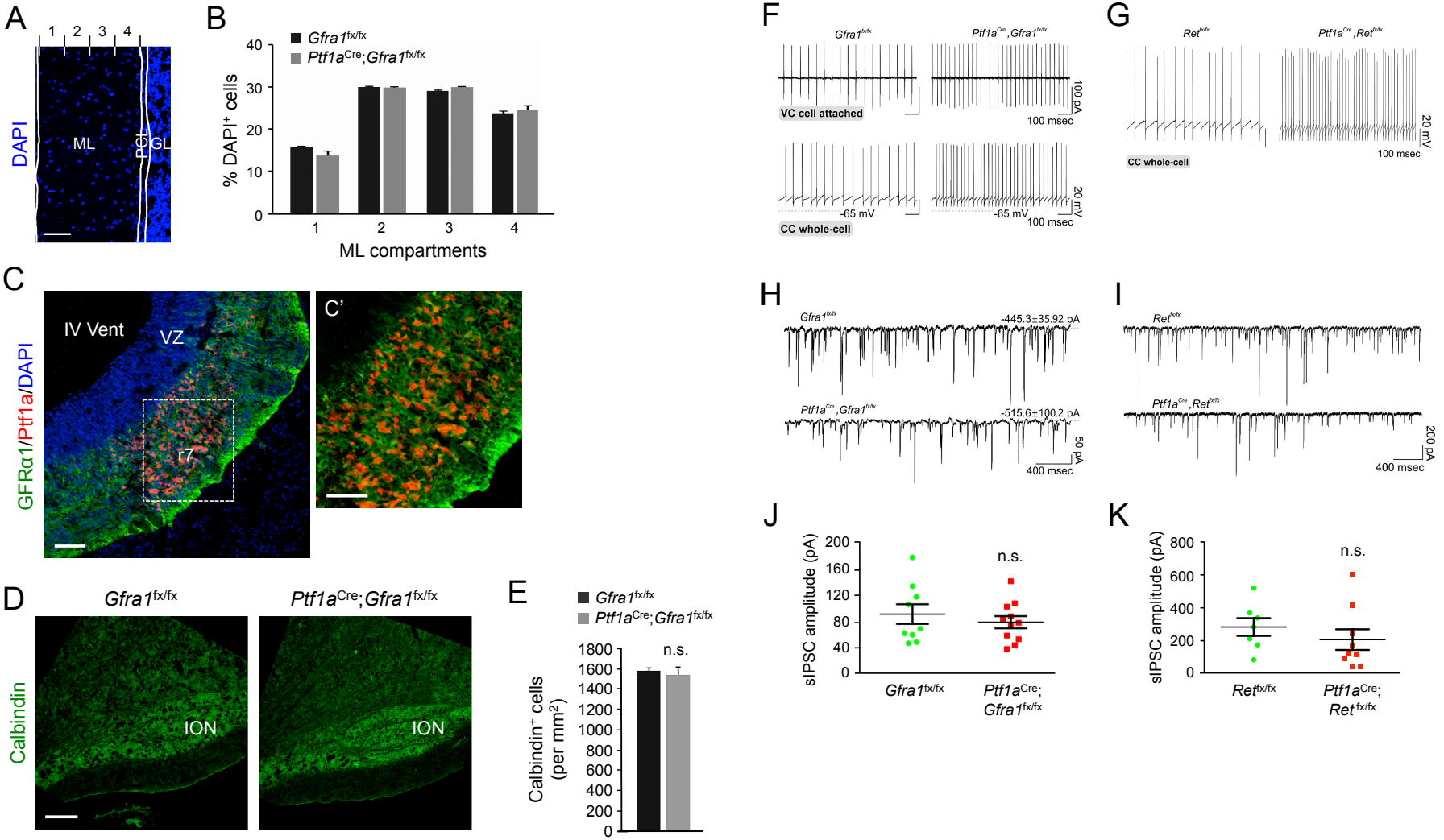

Supplementary Figure S3. Related to Fig. 3. Normal MLI distribution in cerebellum of adult *Gfra1* conditional mutants. Co-expression of GFRα1 and Ptf1a in the embryonic inferior olivary nucleus, but no loss of calbindin positive cells in adult *Ptf1a*^{Cre};*Gfra1*$^{fx/fx}$ conditional mutant mice. Normal MLI distribution and PC sIPSC amplitudes in the cerebellum of adult *Gfra1* and *Ret* conditional mutants

(A) Distribution of DAPI$^+$ cells in the ML of 2 month old *Gfra1* conditional mutant mice and controls. The ML was divided in 4 strata as shown. Scale bar, 50µm.

(B) Quantification of the percentage of DAPI$^+$ cells in each ML stratum. ML: molecular layer, PCL: Purkinje cell layer, GL: granule layer. Values represent mean ± SEM. N=3 mice per group.

(C) Expression of GFRα1 (green) and Ptf1a (red, from *Ptf1a*^{Cre};*Rosa26*^{dTOM}) in E12.5 mouse brainstem. Counterstaining with DAPI in blue. Rostral is to the right. r7, rhombomere 7; IV Vent, IVth ventricle; VZ, ventricular zone. Scale bar, 100µm; inset (C'), 50µm.

(D) Calbindin expression in inferior olivary nucleus (ION) of adult *Ptf1a*^{Cre};*Gfra1*$^{fx/fx}$ conditional mutant mice and *Gfra1*$^{fx/fx}$ control. Scale bar, 100µm.

(E) Quantification of the density of calbindin$^+$ cells in the adult inferior olivary nucleus (ION) of adult *Ptf1a*^{Cre};*Gfra1*$^{fx/fx}$ conditional mutant mice and *Gfra1*$^{fx/fx}$ controls. Values represent mean ± SEM. N=6 mice per group. n.s., not significantly different (p>0.05).

(F) Examples of patch clamp recordings in cell-attached voltage-clamp (top) and whole-cell current-clamp (bottom) modes from PCs in cerebellar slices from *Gfra1*$^{fx/fx}$ (left) and *Ptf1a*^{Cre};*Gfra1*$^{fx/fx}$ (right) mice. Note increased firing frequency in the conditional mutant.

(G) Examples of patch clamp whole-cell recordings from PCs in cerebellar slices from *Ret*$^{fx/fx}$ (left) and *Ptf1a*^{Cre};*Ret*$^{fx/fx}$ (right) mice. Note increased firing frequency in the conditional mutant.

(H) Whole-cell patch clamp recordings from PCs performed in voltage clamp mode from *Gfra1*$^{fx/fx}$ (top) and *Ptf1a*^{Cre};*Gfra1*$^{fx/fx}$ (bottom) mice. Spontaneous inhibitory postsynaptic currents (sIPSCs) were isolated by the application of CNQX and AP-5 to block ionotropic glutamatergic transmission (command potential -60 mV). Note decreased frequency of sIPSCs in mutant mice.

(I) Whole-cell patch clamp recordings of sIPSCs from PCs performed in voltage clamp mode from *Ret*$^{fx/fx}$ (top) and *Ptf1a*^{Cre};*Ret*$^{fx/fx}$ (bottom) mice, performed as described for (H). Note lower sIPSCs frequency in mutant mice.

(J-K) sIPSC amplitude in PCs from cerebella of 2 month old *Gfra1* (E) or *Ret* (F) conditional mutant mice and controls as calculated from whole-cell voltage-clamp recordings in voltage-clamp mode. Each dot represents the mean of values obtained from 300-second recording samples from an individual PC. At least three mice per genotype were used for the recordings. The mean and SEM are shown with parallel lines. N=9 , 11 (J) and 7, 9 (K) PCs per group. n.s: not significantly different.

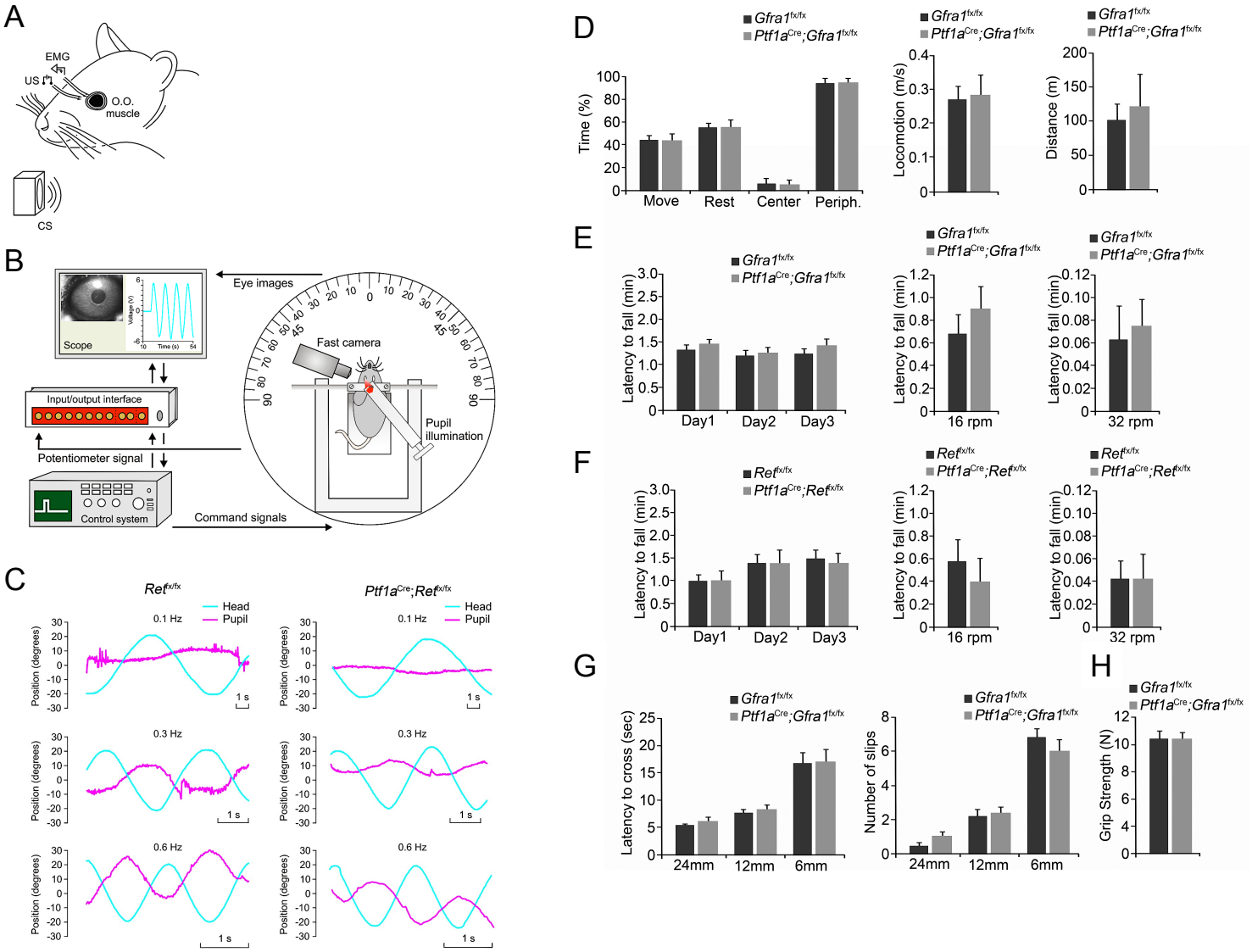

Supplementary Figure S4. Related to Fig. 4. Experimental designs for analysis of classical eyeblink conditioning and vestibulo-ocular reflex. Gfra1 and Ret conditional mutants have normal motor behavior

(A) For classical eyeblink conditioning, animals were presented with a tone as a conditioned stimulus (CS), delivered from a loudspeaker located 50 cm from the animal's head. For unconditioned stimulus (US), mice were implanted with stimulating electrodes on the left supraorbital nerve. To quantify conditioned responses (CRs), mice were implanted with bipolar electrodes to record the electromyographic (EMG) activity of the ipsilateral orbicularis oculi (O.O.) muscle.

(B) For vestibulo-ocular reflex, animals were placed on a turn-table and rotated (± 20°) at three selected frequencies (i.e. 0.1, 0.3, and 0.6 Hz, respectively). Compensatory eye movements were recorded using a fast-camera pupil-tracking system.

(C) Representative examples (averaged 3 times) of vestibulo-ocular (VOR) reflexes evoked in 2 month old *Ret* mutants and controls at the indicated frequencies.

(D) Quantitative analysis of general locomotor behavior of 3 month old *Gfra1*$^{fx/fx}$ and *Ptf1a*^{Cre};*Gfra1*$^{fx/fx}$ mice in the openfield. Histograms show the percent of time spent moving, resting, in center or in periphery (left), the locomotion speed (middle) and the distance covered (right). Histograms show average ± SEM, N=25 mice per group.

(E) Quantitative analysis of rotarod behavior of 3 month old *Gfra1*$^{fx/fx}$ and *Ptf1a*^{Cre};*Gfra1*$^{fx/fx}$ mice. Histograms show the latency to fall off the rod in an accelerating (4-40 rpm, left) and two constant (16 and 32 rpm, middle and right) speed protocols Histograms show average ± SEM, N=25 mice per group.

(F) Quantitative analysis of rotarod behavior of 3 month old *Ret*$^{fx/fx}$ and *Ptf1a*^{Cre};*Ret*$^{fx/fx}$ mice. Histograms show the latency to fall off the rod in an accelerating (4-40 rpm, left) and two constant (16 and 32 rpm, middle and right) speed protocols Histograms show average ± SEM, N=10 mice per group.

(G) Quantitative analysis of behavior of 3 month old *Gfra1*$^{fx/fx}$ and *Ptf1a*^{Cre};*Gfra1*$^{fx/fx}$ mice in the balance beam test using beams of three different sizes as indicated. Histograms show average ± SEM for the latency to cross the beam (left) and the number of slips (right), N=20 mice per group.

(H) Quantitative analysis of the grip strength in Newton (N) of 3 month old *Gfra1*$^{fx/fx}$ and *Ptf1a*^{Cre};*Gfra1*$^{fx/fx}$ mice. Histograms show average ± SEM, N=20 mice per group.

Supplemental Experimental Procedures

Key Resource Table

REAGENT or RESOURCE	SOURCE	IDENTIFIER
Antibodies		
goat anti-GFRα1	R&D	AF560
rabbit anti-Calbindin	Chemicon	AB1778
mouse anti-Calbindin	Swant	#300
rabbit anti-Somatostatin	Peninsula	T-4103
chicken anti-GFP	Abcam	AB13970
rabbit anti-beta galactosidase	Cappel	#55976
rat anti-BrdU	Accurate Chemicals	OBT0030
rabbit anti-Pax2	Invitrogen	#71-6000
rabbit anti.Parvalbumin	Swant	PV25
rabbit anti-Cleaved Caspase3	Cell Signaling	#9661
mouse anti-Dystroglycan	Millipore	#05-298
rabbit anti-Kv1.2	Millipore	AB5924
guinea pig anti-VGAT	Synaptic systems	#131004
donkey anti-goat Alexa Fluor 488	Invitrogen	A11055
donkey anti-goat Alexa Fluor 568	Invitrogen	A11057
donkey anti-rabbit Alexa Fluor 488	Invitrogen	A21206
donkey anti-rabbit Alexa Fluor 555	Invitrogen	A31572
donkey anti-rabbit Alexa Fluor 647	Invitrogen	A31573
donkey anti-mouse Alexa Fluor 488	Invitrogen	A21202
donkey anti-mouse Alexa Fluor 555	Invitrogen	A31570
donkey anti-mouse Alexa Fluor 647	Invitrogen	A31571
donkey anti-rat DyLight 549	Jackson ImmunoResearch	712-506-153
donkey anti-chicken DyLight 488	Jackson ImmunoResearch	703-485-155
donkey anti-guinea pig Alexa Fluor 546	Invitrogen	A11074
Bacterial and Virus Strains		
n. a.		
Biological Samples		
n. a.		
Chemicals, Peptides, and Recombinant Proteins		
4′-6-diamidino-2-phenylindole (DAPI, D1306, Sigma)	Sigma	D1306
Tamoxifen	Sigma	T5648
BrdU	Sigma	B5002
Corn oil	Sigma	C8267
Critical Commercial Assays		
n. a.		
Deposited Data		
n. a.		

Experimental Models: Cell Lines		
n. a.		
Experimental Models: Organisms/Strains		
Mouse: GDNF+/-	Pichel et al., 1996	
Mouse:GDNFbgal/+	Moore et al.,1996	
Mouse:RET GFP/+	Jain et al.,2006	
Mouse:RET fx	Kramer et al., 2006	
Mouse:GFRa1 fx	by Mart Saarma and Jaan-Olle Andressoo	
Mouse:GAD67Cre/+	Tolu et al.,2010	
Mouse:Rosa26YFP/+	Madisen et al.,2010	
Mouse:GFRa1CreERT2/+	Sergaki et al.,2017	
Mouse:Ptf1aCre/+	Kawaguchi et al.,2002	
Oligonucleotides		
n. a.		
Recombinant DNA		
n. a.		
Software and Algorithms		
ImageJ software	http://imagej.nih.gov/ij/	
Matlab scripts	available upon request	
Actimot Software	www.TSE-Systems.com	
GraphPad Prism 6	Graphpad.com	
Other		
n. a.		

Animals

Mice were housed in a 12- hour (h) light/dark cycle and fed a standard diet. The following mouse lines were used: *Gdnf*$^{+/-}$ {Pichel:1996en}, *Gdnf*^{bgal} {Moore:1996io}, *Ret*^{GFP} {Jain:2006ie}, *Ret*^{fx} (Kramer et al., 2006), *Gfra1*^{fx} (kindly provided by Mart Saarma and Jaan-Olle Andressoo, University of Helsinki), *Ptf1a*^{Cre} {Kawaguchi:2002hk}, *Gad67*^{Cre} {Tolu:2010bu}, *Rosa26*^{YFP} {Madisen:2010fi} and *Gfra1*^{CreERT2} {Sergaki:2017uy}. All lines used were in the C57BL/6J background, except *Gdnf*$^{+/-}$ and *Gfra1*^{fx} which were in CD1 background. All studies were performed on mice of both sexes. The day of vaginal plug was considered as embryonic day 0.5 (E0.5) and the day of birth as postnatal day 0 (P0). Control and mutant pups were derived from the same litter. All animal experiments were approved by Stockholm North Ethical Committee for Animal Research (protocols no. N27/15, N173/15 and N26/15).

Histological studies

Postnatal and adult mice were anesthetized with isofluorane and transcardially perfused with PBS followed by 4% PFA. Brains were removed and postfixed in 4% PFA o/n. Tissue samples were washed in PBS, cryoprotected in 20% sucrose at 4°C, embedded

in OCT compound and frozen in dry ice. 14µm sections were obtained across the sagittal plane, collected onto Superfrost Plus slides (Thermo Fischer Scientific), air dried and stored at −20°C until use. For immunostaining, cerebellar sections were blocked for 1h in PBS containing 5% normal donkey serum and 0.1% Triton X-100. Incubation with primary antibodies, diluted in blocking solution, was done o/n at 4°C. The primary antibodies used were as follows: goat anti-GFRα1 (1:200; AF560, R&D), rabbit anti-Calbindin (1:500; AB1778, Chemicon), mouse anti-Calbindin (1:5000; #300, Swant), rabbit anti-Somatostatin (1:500; T-4103, Peninsula), chicken anti-GFP (1:500, AB13970, Abcam), rabbit anti-beta galactosidase (1:500; #55976, Cappel), rat anti-BrdU (1:500, OBT0030, Accurate Chemicals), rabbit anti-Pax2 (1:500, #71-6000, Invitrogen), rabbit anti.Parvalbumin (1:5000; PV25, Swant), mouse anti-Parvalbumin (a:1000; PV235, Swant), rabbit anti-Cleaved Caspase3 (1:500, #9661, Cell Signaling), mouse anti-Dystroglycan (1:500, #05-298, Millipore), rabbit anti-Kv1.2 (1:250; AB5924, Millipore) and guinea pig anti-VGAT (1:250, #131004, Synaptic systems). Sections were washed 3x10minutes (min) in PBS and then incubated with fluorescently labeled secondary antibodies (diluted in blocking solution) and 1µg/ml 4′-6-diamidino-2-phenylindole (DAPI, D1306, Sigma) for counterstaining for 2h at room temperature (R.T). The secondary antibodies used in 1:1000 dilution were as follows: donkey anti-goat Alexa Fluor 488 (A11055) or 568 (A11057, Invitrogen) ; donkey anti-rabbit Alexa Fluor 488 (A21206), 555 (A31572) or 647 (A31573, Invitrogen); donkey anti-mouse Alexa Fluor 488 (A21202), 555 (A31570) or 647 (A31571, Invitrogen); donkey anti-rat DyLight 549 (712-506-153); donkey anti-chicken DyLight 488 (703-485-155, Jackson ImmunoResearch) and donkey anti-guinea pig Alexa Fluor 546 (A11074, Invitrogen). The slides were finally washed 3x10min in PBS and mounted with DAKO fluorescent medium.

Genetic fate mapping and BrdU labeling

For genetic fate mapping, *Gfra1*^{CreERT2};*Rosa26*^{YFP} mice received a single subcutaneous injection of 2mg/30g Tamoxifen (Tmx, Sigma) dissolved in corn oil (Sigma) containing 10% ethanol at P0, P15 and P90.

For BrdU labeling, pups were injected subcutaneously with 25mg/kg BrdU (Sigma) in PBS at P5. Embryos were collected 2h after injection for proliferation analysis or 5 days later for migration studies. For BrdU detection, sections were incubated in 2N HCl, 0.1% Triton X-100 at 37°C for 20min, washed with 0.1M Sodium Borate for 15min, washed 2x5min with PBS and incubated with rat anti-BrdU antibody.

Image analysis

All fluorescent images were captured with a Carl Zeiss LSM710 confocal microscope using ZEN 2009 software (Carl Zeiss) and cell counts were made with ImageJ software (http://imagej.nih.gov/ij/). For caspase-3 analysis, counts were made in the entire length of folial WM from 6 sagittal sections (14 µm thick, one section every 140 µm) per animal from medial to lateral planes. For Pax2 MLI and Golgi cell counts, two images, containing all layers of the cerebellar cortex, were obtained from each folium, approximately at the same location, and 2 midsagittal sections (14 µm) were analyzed per mouse. For counts in adult tissue, DAPI^{+}, PV^{+} cells or Dystroglycan^{+} puncta were analyzed in the molecular layer; Kv1.2^{+} synapses on PC cell bodies.

Cerebellar slice recordings

Cerebellar slices were prepared from 40-50 day-old male and female mice. Following anesthesia with pentobarbital and decapitation, the brain was rapidly removed and

placed in an ice-cold and oxygenated (95%O2/5%CO2) "slicing" solution containing the following: 250mM Sucrose, 26mM NaHCO3, 10mM D(+)□Glucose, 4mM MgCl2, 3mM myo□inositol, 2.5 mM KCl, 2mM Sodium Pyruvate, 1.25mM NaH2PO4, 0.5mM Ascorbic acid, 0.1mM CaCl2 and 1mM Kynurenic acid, pH 7.4. The meninges were gently removed, and the brain was mounted and cut on a vibratome (Leica VT1000). Parasagittal slices (300 µM) were transferred to extracellular artificial cerebrospinal fluid (aCSF): 126mM NaCl, 24mM NaHCO3, 1mM NaH2PO4, 2.5mM KCl, 2.5mM CaCl2, 2mM MgCl2 and 10mM D(+)Glucose, pH 7.4 (osmolarity = 295305 mOsmol). Slices were incubated at room temperature for one hour prior to recording and then transferred to a recording chamber of an upright Axio Examiner D1 Zeiss microscope with infrared differential interference contrast optics that was continuously perfused with aCSF (flow rate = 4ml/min). Whole cell recordings were made from Purkinje cell somata primarily located in lobules 4-7 {Larsell:1952um} at near-physiological temperature (34°C). Whole-cell current- and voltage-clamp recordings were performed with pipettes (2-4 MΩ) made from borosilicate glass capillaries (World Precision Instruments) pulled on a P-97 Flaming/Brown micropipette puller (Sutter Instruments). The holding potential in voltage-clamp recordings was 60 mV. The intracellular recording solution used in experiments contained 140mM Kgluconate, 10mM KCl, 1mM MgCl2, 10mM HEPES, 0.02mM EGTA, 4mM Mg□ATP, 0.4mM Na2□GTP, pH was adjusted to 7.3 with KOH (osmolarity = 278□285 mOsmol).

Recordings of spontaneous inhibitory postsynaptic currents (sIPSCs) were performed in voltage-clamp mode using micropipettes filled with intracellular solution containing (in mM), 150mM KCl, 1mM MgCl2, 10mM HEPES, 0.02mM EGTA, 4mM Mg□ATP, 0.4mM Na2□GTP, pH adjusted to 7.3 with KOH in the presence of 10µM CNQX and 25µM AP-5 to block ionotropic glutamatergic neurotransmission. All sIPSCs recordings were concluded by application of 10µM Gabazine to confirm the GABAergic nature of events by the complete loss of all synaptic currents. Recordings were performed using a Multiclamp 700B amplifier, a DigiData 1440 and pClamp10.2 software (Molecular Devices). Slow and fast capacitative components were automatically compensated for. Access resistance was monitored throughout the experiments, and recordings in which the series resistance exceeded 12 MΩ or changed ≥20% were excluded from further analysis. Liquid junction potential was 9.4 mV and not compensated. The recorded current was sampled at 10 kHz and filtered at 2 kHz. Data analysis was performed with GraphPad Prism6 and custom written Matlab scripts (available upon request). Postsynaptic currents were analyzed using Mini Analysis 6.0.9 (Synaptosoft, Decatur, GA). Detection threshold was set at three-fold the root-meansquare (RMS) noise level, which typically was 3–6 pA. Cumulative frequency was calculated from recordings in voltage clamp mode. Frequency, inter-event-interval, and amplitudes were calculated as a mean of the values obtained from 300-second recording samples. All measurements were taken from at least three mice per genotype.

Behavioral studies

Experiments were carried out on mice of both sexes. *Ret*$^{fx/fx}$ (n = 10) and *Ptf1a*^{Cre};*Ret*$^{fx/fx}$ (n = 8) mice were transferred from the Karolinska Institute in Stockholm to the Pablo de Olavide University in Seville. Animals were housed in individual cages until the end of the experiment on a 12-h light/dark cycle with constant ambient temperature (21 ± 1°C) and humidity (55 ± 5%), with food and water available ad libitum. Experiments were carried out in accordance with the guidelines of the European Union Council (2010/276:33-79/EU) and Spanish (BOE 34:11370-421, 2013) regulations for the use of laboratory

animals in chronic studies, and approved by the local Ethics Committee of the Pablo de Olavide University.

For chronic behavioral studies, mice were anesthetized with 0.8-3% halothane delivered from a calibrated Fluotec 5 (Fluotec-Ohmeda, Tewksbury, MA, USA) vaporizer at a flow rate of 1-2 L/min oxygen. Animals were implanted with bipolar recording electrodes in the left orbicularis oculi muscle and with bipolar stimulating electrodes on the ipsilateral supraorbital nerve. Electrodes were made of 50 µm, Teflon-coated, annealed stainless steel wire (A-M Systems, Everett, WA, USA). Electrode tips were bare of the isolating cover for 0.5 mm and bent into a hook to facilitate a stable insertion in the upper eyelid. Two 0.1-mm bare silver wires were affixed to the skull as a ground. The 6 wires were connected to two 4-pin sockets (RS-Amidata, Madrid, Spain). The sockets were fixed to the skull with the help of 2 small screws and dental cement. A holding system was also fixed to the skull for a proper stabilization during head rotation and eye movement recordings. Further details of this chronic preparation have been explained elsewhere {Gruart:2006fh}.

Classical conditioning was achieved using a delay paradigm (Figure S4A). Animals (6 at a time) were placed in separate small (5x5x10 cm) plastic chambers located inside a larger (35x35x25 cm) Faraday box. As conditioned stimulus (CS) animals were presented with a tone (2.4 kHz, 85 dB) lasting for 350 ms. The unconditioned stimulus (US) consisted of a cathodal, square pulse applied to the supraorbital nerve (500 µsec, 3 x threshold) at the end of the conditioned stimulus. A total of 2 habituation, 10 conditioning, and 5 extinction sessions were carried out for each animal. A conditioning session consisted of 60 CS-US presentations and lasted 30 min. For a proper analysis of the evoked conditioned responses, the conditioned stimulus was presented alone in 10% of the cases. Paired conditioned stimulus-unconditioned stimulus presentations were separated at random by 30 ± 5 sec. For habituation and extinction sessions, only the conditioned stimulus was presented, also for 60 times per session, at intervals of 30 ± 5 sec. Training sessions lasted for about 30 min {Gruart:2006fh}. Unrectified EMG activity of the orbicularis oculi muscle, and 1-V rectangular pulses corresponding to conditioned and unconditioned stimuli were stored digitally in a computer through an analog/digital converter (1401-plus; CED; Cambridge, UK) for quantitative off-line analysis. Collected data were sampled at 10 kHz for EMG recordings, with an amplitude resolution of 12 bits. A computer program (Spike2 from CED) was used to display the EMG activity of the orbicularis oculi muscle.

For vestibular stimulation, a single animal was placed on a home-made turning-table system (Figure S4B). Its head was immobilized with the help of the implanted holding system, while the animal was capable to walk over a running wheel. Table rotation was carried out by hand following a sinusoidal display in scope. Actual rotation of the table was recorded with a potentiometer attached to the rotating axis. The animal was rotated by ± 20º at three selected frequencies (0.1, 0.3, and 0.6 Hz) for about ten cycles with intervals of 2 min between frequencies. Recording sessions were repeated three times per animal. The eye of the mouse was illuminated with an infrared emitter (wavelength: 880 nm) attached to the head holding system. Eye positions during head rotation were recorded with a fast infrared CCD camera (Pike F-032, Allied Technologies, Stadtroda, Germany) at a rate of 60 pictures/sec. Eye positions for each frequency and animal were averaged (10 complete rotations x 3 recording sessions) for offline analysis of gain and phase {deJeu:2012hc}. The number of compensatory eye saccades were also quantified as it is known improper performance of the VOR are partially compensated by eye

saccades {Macdougall:2012fi}. Head and eye positions were stored digitally in the same analog/digital converter and processed off-line with the help of a MATLAB based (MathWorks, Natick, MA) home-made tracking program. Gain was computed as the ratio between the changes in pupil and head angles during a head turn. Phase was computed as the angle difference between head and pupil.

Open field behavior was investigated with the TSE Actimot system (www.TSE-Systems.com) composed of 480 x 480mm transparent acrylic boxes equipped with light-beam strips to record locomotor behavior. Mice of each genotype 2-3 months old were tested for 15 min without habituation (25 mice per genotype for *Ptf1a*^{Cre};*Gfra1*$^{fx/fx}$ mutants and 10 mice per genotype for *Ptf1a*^{Cre};*Ret*$^{fx/fx}$ mutants). Actimot Software was used to calculate general locomotion parameters, including distance travelled, speed, rearing events and wall-hugging behavior.

For the rotarod test, mice 2–3 month old were first habituated for 1 min to a rotarod apparatus equipped with automatic fall detector rotating at 4 rpm. Mice were then trained in accelerating speed (4 to 40 rpm) during 3 trials 15 min apart per day on 3 consecutive days. The latency to fall from the rod was registered and best daily performance of each animal was recorded for analysis. A trial was otherwise terminated if the animal rotated passively with the rod or after 5 min. One day after the training period, mice were subjected to a steady speed trial (16 or 32 rpm) and the latency to fall was recorded as above for 3 trials per animal. Again the best score for each mouse was used.

For the balance test, animals were required to sequentially traverse three horizontal elevated narrow beams of different thicknesses starting from the thickest (24mm) to medium (12mm) and finally to the thinest (6mm). The beams were 1m long and were supported on vertical poles (50cm high). A soft pad was put under the beam in case the animal fell off. A cage with bedding material covered with a black blanket was placed on the one edge of the beam. Each mouse was placed on the free edge of the beam and the latency to reach the cage as well as the number of slips was recorded. Two trials per mouse were performed for each beam. If the mouse failed to cross the beam within 5 min the trial was aborted.

Statistical analysis

All experiments were performed blind to the genotype until the end of the analysis. Experimental groups were subsequently generated according to mice genotype without any randomization. The variation between groups was automatically calculated by GraphPad Prism 6 and was similar between groups.

For image analysis, Student's t-test was used for evaluation of the statistical significance of the results. All data are presented as means ± standard error of the mean (SEM). Significance levels are indicated as: * = $p<0.05$; ** = $p<0.01$ and *** = $p<0.001$.

For slice recordings, two-sample Kolmogorov-Smirnov (K-S2) test was used to compare pooled cumulative frequency distributions. Otherwise, statistical significance was set at $p<0.05$ and was determined using the appropriate two-tailed Student's t-test. All data are presented as means ± SEM. Significance levels are indicated as: * = $p<0.05$; ** = $p<0.01$ and *** = $p<0.001$.

For behavioral studies, statistical analyses were carried out using the SPSS package (SPSS Inc., ILL, USA) for a statistical significance level of $p<0.05$. Unless otherwise indicated, mean values are followed by SEM. Collected data were analyzed using a two-

way ANOVA test, with time or session as repeated measure, coupled with contrast analysis when appropriate. When necessary, the Student's t-test was used for the comparison between two independent means and the paired t-test when related to the same measurements.